Universal cross sections for K-shell ionization by heavy charged particles. II. Intermediate particle velocities

George Basbas,* Werner Brandt, and Roman Laubert
Department of Physics, New York University, New York, New York 10003
(Received 2 May 1977)

Experimental K-shell ionization cross sections of $_{13}$Al and $_{28}$Ni are reported for ions of $^{1}_{1}$H, $^{2}_{1}$H, $^{4}_{2}$He, $^{6}_{3}$Li, and $^{7}_{3}$Li with kinetic energies in the range from 2 to 36 MeV, and of $_{28}$Ni for ions of $^{12}_{6}$C, $^{16}_{8}$O, and $^{19}_{9}$F in the range from 4 to 90 MeV. The theory of direct Coulomb K-shell ionization, as developed in an earlier paper [Phys. Rev. A 7, 983 (1973)] for projectiles of atomic number Z_1, small compared to the target atomic number Z_2, and of velocities v_1 small compared to the target K-shell electron velocity v_{2K}, i.e., $v_1 \ll v_{2K}$, is extended to intermediate velocities $v_1 \simeq v_{2K}$. New effects appear. They add to the Z_1^2-proportional cross sections one derives from linear-response theories for direct ionizations. They are attributed to the polarization of the target K shell in the field of the projectile, and to electron capture by the projectile. Guided by the perturbed stationary-state theory of atomic collisions, the polarization effects are incorporated so that the theory retains the unifying aspects of the cross sections derived in the plane-wave Born approximation, but the variables now contain the nonlinear effects as scaling factors. Electron-capture cross sections are added. When $v_1 \gg v_{2K}$, such contributions subside, and one retrieves the cross sections of the linear-response approximation. The theory predicts K-shell ionization cross sections for projectiles with $Z_1/Z_2 < 0.5$ at all velocities in a comprehensive manner. It agrees with experimental data covering six orders of magnitude for collisions partners with Z_1/Z_2 ranging from 0.03 to 0.3 and v_1/v_{2K} from 0.07 to 2.

I. INTRODUCTION

This is the second of two papers on the Coulomb excitation of K shells in atoms during collisions with heavy charged particles. The heavy particle refers to projectiles of mass M_1, large compared to the electron mass m, and of atomic number Z_1, small compared to the atomic number Z_2, of the target atoms. The projectile K-shell radius is large compared to the interaction region for the K-shell excitation of the target atom in slow collisions, and the moving projectile acts as a bare point charge with regard to this process, unencumbered by the coterie of bound electrons it may carry into the collision. The first paper,[1] labeled KI, treats slow collisions. Slow collisions pertain to regime I of particle velocities v_1 that are small compared to the mean orbital velocity in the target K shell v_{2K}. In short, KI describes K-shell ionizations by charged particles under the conditions $m \ll M_1$, $Z_1 \ll Z_2$, and $v_1 \ll v_{2K}$. In a paper[2] labeled LI, the ionization of L shells is investigated in this regime.

Formulations of Coulomb excitation in the quantum-mechanical, plane-wave Born approximation (PWBA) or the classical, binary-encounter approximation (BEA) are linear-response theories. They do not treat effects of the perturbation on the states between which the transitions occur, and result in ionization cross sections proportional to Z_1^2. In the low-velocity regime I, subtractive effects of binding and Coulomb deflection reduce cross sections significantly, at times by as much as two orders of magnitude relative to the predictions of the linear-response theories. Our approach to inner-shell ionizations by heavy charged particles in the framework of the perturbed stationary-state (PSS) theory[3,4] allows *ab initio* for such effects in its basis states, and predicts the K- and L-shell ionization cross sections in regime I correctly, as demonstrated in KI and LI.

The present paper, labeled KII, extends the theory to collisions in intermediate particle-velocity regime II, where v_1 becomes comparable to v_{2K} and the effects of Coulomb deflection of the projectile trajectory by the target nucleus become small. That is, we describe direct Coulomb K-shell ionizations by charged particles under the conditions $m \ll M_1$, $Z_1 \ll Z_2$, and $v_1 \lesssim v_{2K}$. New effects appear due to the polarization of the K shell by the field of the moving particle. They are not contained in approximations based on unperturbed states, e.g., in the PWBA. We report measurements pertaining to the polarization effect and present details of the comprehensive theory of K-shell ionization cross sections presented earlier.[3] The theory is based on time-dependent adiabatic atomic states that are perturbed by a projectile with a classical trajectory. Expansion of the ionization-probability amplitude about the instant of closest approach leads to a formulation in terms of perturbed stationary states (PSS).[4] Our treatment as given in KI and the present KII includes Coulomb deflection (C) of

the projectiles and may be labeled CPSS. It differs at its very inception from the PWBA and the usual semiclassical approximation (SCA) which use unperturbed basis sets. Cross sections so derived predict accurately the experimental data in regimes I and II, ranging in v_1/v_{2K} from 0.07 to 2.

In regime III of high velocities $v_1 \gg v_{2K}$, not reached here experimentally, polarization effects subside, and the cross sections become asymptotically proportional to Z_1^2.[5]

Our approach is guided by a "universal" viewpoint; to wit, it summarizes what is known about inner-shell ionization under Coulomb excitation conditions in a comprehensive manner. This permits one to juxtapose and to test the consistency of data from different systems on a common basis. New phenomena are uncovered and gauged in proper perspective as deviations from the unified reference curve. In successive approximations, the unified approach reflects the similitude in the underlying atomic processes, and culls timely problems worthy of concerted efforts.

The PSS formulation casts the problem of direct inner-shell ionization to the continuum in the terms of a semiclassical theory. Binding and polarization effects on target states by the projectile charge are an innate part of the PSS theory. One retrieves the mathematical form of the SCA ionization probability, but with the distinctly novel content that the target states are perturbed. The development permits one to incorporate nonlinear-response effects into the PWBA cross sections through appropriate scaling of the variables. This has the serendipitous consequence that one may use the extensive numerical tabulations available for PWBA K- and L-shell cross sections[6,7] in applications of the CPSS theory. The PWBA is contained in the PSS framework as a special case valid only under very limiting conditions which, in general, are not fulfilled in the Coulomb ionization of inner atomic shells by swift charged particles.[1]

In velocity regime II of our present concern, the projectile traverses the K shell, of radius a_{2K}, in times a_{2K}/v_1 comparable to the orbital period of the K shell ω_{2K}^{-1}, where $\hbar\omega_{2K}$ is the electron binding energy in the shell. The minimum momentum transfer $\hbar q_0 \equiv \hbar\omega_{2K}/v_1$ necessary for the ionization of an unperturbed K shell implies that $q_0^{-1} \simeq a_{2K}$ when $v_1 \simeq v_{2K}$. Since the dominant contribution to ionization in velocity regime II is made by projectiles at impact parameters $b \sim q_0^{-1}$, the important interaction range is comparable to the K-shell radius, $b_{\text{important}} \simeq a_{2K}$, and the central parameter of the theory

$$\xi_K \equiv (q_0 a_{2K})^{-1} = v_1/\tfrac{1}{2}\,\Theta_K v_{2K} \qquad (1)$$

has values of the order of 1. The low velocities of regime I refer to the limit $\xi_K \ll 1$, and the high velocities of regime III to $\xi_K \gg 1$. For later reference, we define the conventional parameter

$$\eta_K \equiv (v_1/v_{2K})^2 = v_1^2/Z_{2K}^2 v_0^2 = (\tfrac{1}{2}\,\Theta_K)^2 \xi_K^2 , \qquad (2)$$

which is proportional to the kinetic energy E_1 per mass M_1 of the projectile, E_1/M_1. For a target at rest in the laboratory, v_1 is the beam velocity. Here and in the following, we place $a_{2K} = a_0/Z_{2K}$, where $a_0 = 1$ a.u. $= \hbar^2/me^2 = 0.529$ Å is the Bohr radius, and set $Z_{2K} = Z_2 - 0.3$. The electron binding energy $\hbar\omega_{2K}$ is expressed in terms of the dimensionless parameter $\Theta_K \equiv \hbar\omega_{2K}/Z_{2K}^2 \mathcal{R}$, where $\mathcal{R} = \frac{1}{2}$ a.u. $= e^2/2a_0 = 13.6$ eV. This parameter measures the nonhydrogenic character of the K-shell ionization energy and ranges from 0.6 in light elements to 0.9 in the heaviest elements. The mean hydrogenic K-shell orbital velocity is $v_{2K} = Z_{2K} v_0$, $v_0 = 1$ a.u. $= e^2/\hbar$ $= 2.18 \times 10^8$ cm/sec being the Bohr velocity. If M_1 is given in atomic mass units (amu), η_K relates to E_1 as

$$\eta_K \simeq 40[E_1(\text{MeV})/M_1] Z_{2K}^{-2} , \qquad (3)$$

and ξ_K becomes

$$\xi_K \simeq \sqrt{160}\,[E_1(\text{MeV})/M_1]^{1/2} (\Theta_K Z_{2K})^{-1} . \qquad (4)$$

Section II presents new data on ionization cross sections determined through measurements of characteristic x-ray yields in thin-target transmission experiments. The data exhibit K-shell polarization effects and electron-capture contributions. Polarization effects are introduced in Sec. III in terms of a treatment developed for similar effects in the stopping power of targets for swift charged particles.[8] Section IV compares the theory with the experiments in a comprehensive manner. The conclusions are summarized in Sec. V. The Appendix presents an illustrative numerical example for the calculation of K-shell ionization cross sections in velocity regime II.

II. NEW DATA

We report thin-target measurements of characteristic K-shell x-ray yields for $_{13}$Al and $_{28}$Ni targets excited by ions of $^1_1$H, $^2_1$H, $^4_2$He, $^6_3$Li, and $^7_3$Li in the energy range from 2 to 36 MeV, and for $_{28}$Ni targets excited by ions of $^{12}_{6}$C, $^{16}_{8}$O, and $^{19}_{9}$F in the range from 4 to 90 MeV. Together with the measurements reported in K I, these data test our theory of direct K-shell ionization by heavy charged particles in the velocity regimes I and II in a consistent manner.

A. Experiments with $1 \leq Z_1 \leq 3$ on $_{13}$Al and $_{28}$Ni

Ion beams, generated with 20–50 nA of current in the tandem Van de Graaff accelerator of the Brookhaven National Laboratory, were collimated by two circular 0.25-mm-diam apertures placed 30 cm apart in front of the target. A series of aluminum and nickel target foils were mounted on a ladder and placed in a 76-cm-diam scattering chamber in such a way that they were tilted 45° with regard to both the beam direction and the line of sight of the x-ray detector. The transmitted beam intensity was measured in a 10-m-long Faraday cup with a 10-cm-diam aperture placed 40-cm downstream from the target. The target was biased at +1 kV to retain secondary electrons and the Faraday cup aperture at −1 kV to prevent electron escape to the target.

The target thickness was monitored by the yield of beam particles scattered in the target through 35° into a 50-mm^2 solid-state detector positioned 16 cm from the target. The x rays were recorded in a 30-mm^2 Si(Li) x-ray detector, placed 80 cm from the target, separated from the target vacuum system by a 25-μm-thick Be window, and shielded by a 2-cm-thick lead cylinder from the high-energy γ rays produced at the collimators. The detector resolution function, as measured with Fe($K\alpha$) x rays from a ^{57}Co γ calibration source, had a full width at half maximum of 240 eV.

The output pulses from the x-ray and particle detector amplifiers were stored separately, each in 1024 channels of a 4096-channel pulse-height analyzer (PHA). The beam current collected in the Faraday cup was digitized and counted by a scaler that gated the PHA.

Despite the lead shielding, many saturated pulses were transmitted randomly by the x-ray detector amplifier, causing "ringing" for 50–100 μsec. Such pulses were excluded by letting them turn off the x-ray PHA through an upper-level discriminator, set at 10 keV, coupled to a 110-μsec shaper whose output was fed into the anticoincidence mode of the x-ray PHA. This device maintained a peak-to-background ratio of ca. 10^2 in the vicinity of the characteristic x-ray peaks.

The energy spectra of the Al(K) and Ni(K) x rays were found to be independent of the particles and their velocities, as was the ratio of the $K\beta$ to $K\alpha$ yields in Ni. The value of this ratio 0.133 ± 0.005 agrees with previous measurements[9] and with theory.[10,11] We conclude that the x-ray fluorescence yields were constant under our conditions.

The count of x rays for a preset collected amount of beam charge was reproducible to 1%, even over 24-h periods of operation with some 100 movements of the target ladder.

To calculate absolute x-ray yields from these data, the detector efficiency, including the transmission of the Be window, the gold surface layer, and the Si deadlayer, was determined to be 0.39 ± 0.02 for Al(K) x rays and 0.97 ± 0.05 for Ni(K) x rays.[12] Measurement of the Rutherford-scattered particle flux contributed a 6% uncertainty in the target thickness t of Al ($\simeq$23 μg/cm^2) and Ni ($\simeq$180 μg/cm^2) targets. The scattering cross sections differed by less than 3% from the Rutherford cross sections, as judged by calculations based on the optical model of the target nuclei.[13] The propagation of random errors attaches an uncertainty of 10% to the absolute x-ray yields. The uncertainties of relative yields measured for a particular target are $\simeq$1.5%. By comparison, relative yields for thick targets carry uncertainties of 20%–30%.

B. Experiments with $6 \leq Z_1 \leq 9$ on $_{28}$Ni

When $Z_1 \geq 6$, the charge states of the transmitted projectiles in our velocity range are uncertain, and the beam currents collected are no longer reliable indicators of the number of incident particles. Therefore, we counted the number of projectiles, N_s, scattered from the target of thickness t concurrently with the number of x rays, N_x, emanating from the target. At the beginning of each run, N_s was recorded as a function of the scattering angle and a particle-detector orientation chosen such that the counts were accumulated under conditions of proper Rutherford scattering so that N_s was proportional to $N_i t$, N_i being the number of incident projectiles. This required measurements at scattering angles ranging between 8° and 45°, depending on the projectile-target combination in a given run.

In contrast to our observations with $Z_1 \leq 3$, the Ni(K) x-ray spectra change with the atomic number Z_1 and the velocity v_1 of the incident particles. Aside from the $K\alpha$ and $K\beta$ transitions, three resolved and possibly two or more unresolved x-ray transitions were observed near 1.2, 2.0, and 2.8 keV, with intensities comparable to the Ni($K\alpha$) line intensity. The low-energy x-ray bands are mirrored in the proton-excited spectra, but they amount there to only 2% relative to the Ni($K\alpha$) intensity. They may originate from transitions excited in target impurities, from molecular-orbital transitions during collisions of recoil atoms in the target, and from radiative electron capture by the projectiles. The intensities of 2.0- and 2.8-keV bands rise relative to that of the 1.2-keV band with increasing ion energies. The charge state of the incident ions had no measurable effect on the

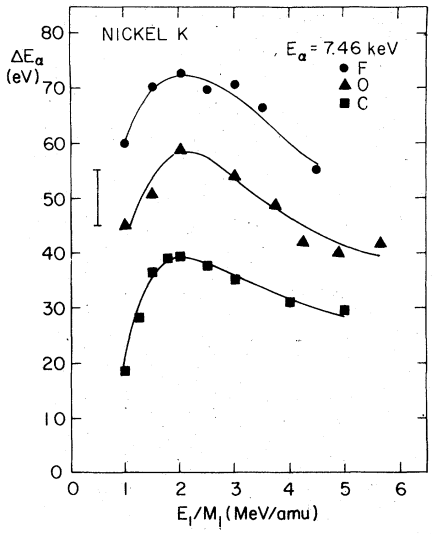

FIG. 1. Observed $_{28}$Ni($K\alpha$) x-ray energy shift ΔE_α, relative to proton excitation, for $^{12}_{6}$C, $^{16}_{8}$O, and $^{19}_{9}$F projectiles as a function of their kinetic energy per nucleon. The error bar marks the uncertainty in the absolute scale.

low-energy x-ray bands, or on the measured x-ray production cross sections. For ions with $Z_1 > 3$, the energies of the Ni(K) x rays shift to higher values with increasing velocity and atomic number of the ionizing projectiles. The increment ΔE_α of the Ni($K\alpha$) x-ray energy relative to the x-ray spectrum excited with protons at equal velocity is shown in Fig. 1. The rise of the Ni($K\beta$) x-ray energy is twice as large, with a similar velocity dependence. The ratio of $K\beta$-to-$K\alpha$ yields, Y_β/Y_α, varies with v_1 as depicted in Fig. 2. The dashed line represents an average of some 100 measurements with particles $Z_1 < 3$. For $6 \leq Z_1 \leq 9$, the ratio increases to a maximum near $E_1/M_1 = 2.5$ MeV/amu and declines slowly at higher energies. Similar shifts and variations of the yield ratios are known to occur for $^{16}_{8}$O on $_{26}$Fe and $_{29}$Cu targets.[14-16]

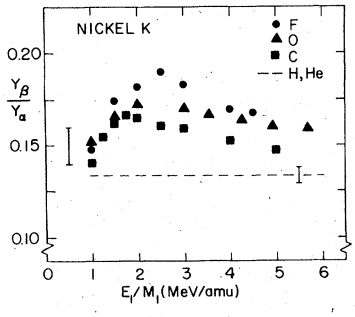

FIG. 2. Ratio of $K\beta$ yield, $Y\beta$, and $K\alpha$ yield, $Y\alpha$, of $_{28}$Ni(K) x rays for $^{12}_{6}$C, $^{16}_{8}$O, and $^{19}_{9}$F projectiles as a function of their kinetic energy per nucleon. The dashed line represents the measurements with $^{1}_{1}$H and $^{4}_{2}$He projectiles. The error bar marks the uncertainty in the absolute scale.

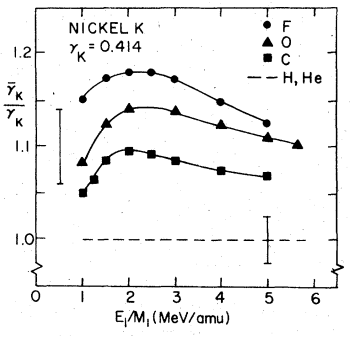

FIG. 3. Variation in the fluorescence yield ratio $\bar{\gamma}_K/\gamma_K$ of $_{28}$Ni x rays for $^{12}_{6}$C, $^{16}_{8}$O, and $^{19}_{9}$F projectiles, as a function of their kinetic energy per nucleon, relative to $\gamma_K = 0.41$, applicable to $^{1}_{1}$H, $^{4}_{2}$He, and $^{6,7}_{3}$Li projectiles. The error bars mark the uncertainties in the absolute scale.

The observations are consistent with changes in the outer screening owing to vacancies produced in other shells concomitantly with a K-shell vacancy. The fluorescence yield for the emission of K-shell x rays in the presence of vacancies in other shells, $\bar{\gamma}_K$, exceeds the yield, γ_K, obtained when all other shells are filled. Using the fractional-parentage coefficient method,[17] one can calculate $\bar{\gamma}_K$ relative to[18] $\gamma_K = 0.41$ under the assumption that vacancies in the L shells are the main cause for the x-ray energy shifts and yield-ratio variations, with the result shown in Fig. 3. The dashed line $\bar{\gamma}_K = \gamma_K$ reflects our experimental findings for $Z_1 \leq 3$.

C. Data analysis

A particle of kinetic energy E_1, entering a foil of thickness t tilted at angle θ relative to the foil normal, traverses an effective sample thickness $t' = t/\cos\theta$. The yield Y(x rays/particle) of x rays emanating from the foil is given by

$$Y = n \int_0^{t' \leq R_0(E_1)} e^{-az} \sigma_x [E(R_0 - z)]\, dz\,, \qquad (5)$$

where n is the atomic density of the target material; $R_0(E_1)$ is the projected particle range; $a = \mu(\cos\theta/\cos\phi)$ depends on the mass absorption coefficient μ of the medium for its K-shell x rays and the angles from the normal to the foil of particle incidence θ and x-ray detection ϕ; $\sigma_x[E(R)]$ is the x-ray production cross section per target atom for the projectiles of energy $E(R)$ with residual range $R = R_0(E_1) - z$, and z the path length in the target. Differentiation of Eq. (5)

with regard to $E_1 = E(R_0)$ gives

$$\sigma_x(E_1) - e^{-at'}\sigma_x[E(R_0 - t')] = n^{-1}[S(E_1)(dY/dE_1) + aY], \quad t' \leq R_0(E_1) \tag{6}$$

in terms of the target stopping power $S(E_1) = [dR_0(E_1)/dE_1]^{-1}$. In the thick-target limit with yield Y_{th}, one retrieves Eq. (3) of K I,

$$\sigma_x(E_1) = n^{-1}[S(E_1)(dY_{th}/dE_1) + aY_{th}(E_1)]. \tag{7}$$

For energy losses $\Delta E = E_1 - E(R)$ in thin targets, $t' \ll R_0(E_1)$, such that $\Delta E \simeq S(E_1)t' \ll E_1$, we expand σ_x, Eq. (5), about $z = 0$ and integrate term by term,

$$Y = n\frac{1 - e^{-at'}}{a}\left(\sigma_x(E_1) - \frac{d\sigma_x(E)}{dE}\bigg|_{E=E_1} \times \overline{\Delta E}(t') + \cdots\right), \tag{8}$$

where

$$\overline{\Delta E}(t') \equiv \tfrac{1}{2} S(E_1)t' f(at'), \tag{9}$$

with the abbreviation

$$f(x) = 2\frac{1 - (1+x)e^{-x}}{x(1 - e^{-x})} \leq 1,$$

which is bounded by $f(0) = 1$. For thin targets, so that $\overline{\Delta E} \simeq \frac{1}{2}\Delta E \ll E_1$, summing Eq. (8) as a Taylor expansion in $\overline{\Delta E}$ gives

$$Y = nt'\frac{1 - e^{-at'}}{at'}\sigma_x(E_1 - \overline{\Delta E}). \tag{10}$$

If the target is tilted while the angle between beam direction and x-ray detector remains constant, $\theta + \phi = \text{const}$, Y may be treated as a function of θ. By expanding Eq. (10) for small $\overline{\Delta E}$ in the limit $a = 0$, i.e., when self-absorption is negligible ($\mu = 0$), the yield may be approximated by

$$Y = Ay - By^2 + C, \tag{11}$$

where

$$y = (\cos\theta)^{-1}, \tag{12}$$

$$A = nt\,\sigma_x(E_1), \tag{13}$$

$$B = \tfrac{1}{2} nt^2 S(E_1)[d\sigma_x(E)/dE]_{E=E_1}, \tag{14}$$

and C may be some θ-insensitive background not included in Eq. (10).

We have performed a series of experiments by varying θ at constant t to ascertain the merits of Eq. (11) for determining $\sigma_x(E_1)$ from A through formal extrapolations of the values of $(Y - C)/y$, measured as a function of $y \equiv (\cos\theta)^{-1} \geq 1$, to $y \to 0$. Figure 4 shows the result of a typical run on Al with 250-keV protons, where the target-thickness

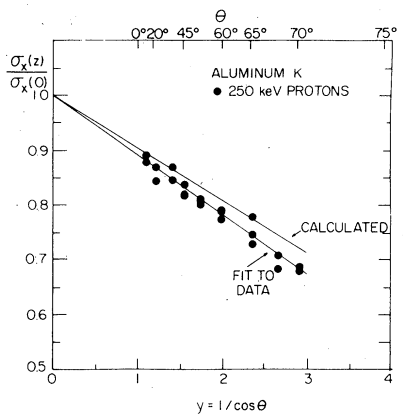

FIG. 4. Al(K) x-ray production cross sections from a 27 μg/cm^2 Al foil as a function of $y = 1/\cos\theta$, where θ is the tilt angle. Formal extrapolation to $y = 0$ yields the thin-target cross section. The ordinate presents $1 - (B/A)y$. The curve labeled "calculated" was obtained from Eqs. (11) and (14) with best available estimates for the required physical quantities. The deviation from the data reflects uncertainties associated with the values inserted into Eq. (14). The crux of the tilt method is that Eq. (14) does not need to be consulted to obtain the cross section.

correction is relatively large ($\simeq$10%). We find that the target-tilt technique determines the cross section $\sigma_x(E_1)$ accurately in velocity regime I without explicit knowledge of the stopping power. However, in the x-ray production experiments in velocity regime II reported here, the tilt technique offers no significant improvements commensurate with the many measurements required to determine the cross section at a particular energy. Instead, we set

$$\sigma_x(E_1) = \cos\theta\, Y(E_1)/nt, \tag{15}$$

and extract $Y(E_1)$ from the experimental yields Y_{exp} as given in Eq. (16) below, which includes small calculated rather than empirical target-thickness corrections. Under our conditions, at $\theta = 45°$ and with target surface densities $\rho = td/\cos\theta$, d being the mean density of the material, one obtains (1 b = 10^{-24} cm^2)

$$\sigma_x(E_1)(b) = k\frac{Y(E_1)\ (\text{x rays/particle})}{\rho\ (\mu\text{g/cm}^2)},$$

where k(Al) = 4.48×10^7 (μg b/cm^2) and k(Ni) = 9.75×10^7 (μg b/cm^2).

The measured yields contain contributions that are not included in Eq. (5), but may be subsumed in the constant C of Eq. (11). One contribution, Y_{rec}, stems from cascades of recoiling atoms set in motion by the projectiles; another, Y_{sc}, is added by projectiles that undergo large-angle scattering on target atoms and have path lengths in the target

significantly in excess of the target thickness.

Briefly, the measured x-ray yields $Y_{exp}(E_1)$ can be related to the relevant characteristic x-ray yields of target atoms produced by the projectiles, $Y(E_1)$, as

$$Y = Y_{exp}\,\frac{\alpha_{sc}}{\alpha_x}\left(1-\frac{Y_{rec}+Y_{sc}}{Y_{exp}}\right). \tag{16}$$

The coefficients

$$\alpha_{sc}=\left(1-\frac{\overline{\Delta E}_R}{E_1}\right)^{-2},\quad \alpha_x=\frac{1-e^{-at'}}{at'}\left(1-\frac{\overline{\Delta E}}{E_1}\right)^{l},$$

in terms of Eq. (9) $\overline{\Delta E}_R=\Delta\overline{E}(a=0)$, correct the Rutherford-scattering and x-ray counts for the mean-energy loss in the target of thickness t'. They follow, respectively, from the E^{-2} dependence of the Rutherford-scattering cross section used to calculate the number of incident particles and from the dependence $\sigma_x = cE^l$ of the x-ray production cross sections of projectile energy E, where c and l are suitable constants. Recoiling target atoms contribute[19]

$$Y_{rec}=n^2t'\int_{T_{min}}^{T_{max}}\frac{d\sigma(T)}{dT}\,dT \times\int_{T-t''S_{22}}^{T} e^{-a(R_0(E_1)-R(E))} \times\sigma_x(Z_2,Z_2,E)S_{22}^{-1}(E)\,dE, \tag{17}$$

where t'' is the exit path length of the recoiling target atom and $d\sigma(T)/dT$ is the differential cross section for the transfer of energy T from the projectile to a target atom with T ranging from some T_{min} to $T_{max}=4M_1M_2E_1/(M_1+M_2)^2$; $\sigma_x(Z_2,Z_2E)$ denotes the x-ray production cross section for target atoms moving at energy E in the target with stopping power $S_{22}(E)$. As discussed earlier,[19] we set

$$\sigma_x(Z_2,Z_2,E)=A(1-B/E)\theta(B-E), \tag{18}$$

where

$$A=\gamma_K P\pi r_c^2,$$

$$B=2Z_2^2e^2r_c^{-1}\exp(-2^{1/2}Z_2^{1/3}r_c/a_0)\geq T_{min},$$

$$\theta=\tfrac{1}{2}(1+x/|x|),$$

with $P\simeq 0.1$ and $r_c\simeq a_0Z_2^{-1}$. On integration, one obtains

$$Y_{rec}=5.45\times10^{-21}n^2t'^2A\left(\frac{Z_1Z_2(M_1+M_2)}{M_2E_1}\right)^2 \times\left[\frac{2}{5}\left(\frac{T_{max}}{B}\right)^{3/2}+\frac{3}{5}\left(\frac{T_{max}}{B}\right)^{-1}-1\right], \tag{19}$$

if A is given in cm^2 and E_1 in keV. Equation (19) is the thin-target analog of Eq. (14) in Ref. 19. In this approximation, Y_{rec} has a threshold at

$$E_1/M_1\simeq 1.84\times10^{-2}Z_2^3(M_1+M_2)^2/M_1^2M_2\ (\text{keV/amu}).$$

As E_1 increases, Y_{rec} passes through a maximum and then decreases as $E_1^{-1/2}$.

Primary projectiles scattered through angles larger than 10° have discernibly longer paths and contribute to the x-ray yield in thin targets according to

$$Y_{sc}=1.6\times10^{-17}n^2t'^2(Z_1Z_2/E_1)^2 \times\left(\frac{\sigma_x(Z_1,Z_2,E_1')}{\cos\beta}-\sigma_x(Z_1,Z_2,E_1)\right). \tag{20}$$

The energy of the scattered particle is denoted E_1' and is given by

$$E_1'=\frac{E_1M_1^2}{(M_1+M_2)^2}\left[\cos\beta+\left(\frac{M_2^2}{M_1^2}-\sin^2\beta\right)^{1/2}\right]^2.$$

Evaluation of E_1' utilized a value of 17° for the scattering angle β. This number corresponds to the average value of $\cos\beta$, weighted by the Rutherford cross section, over the range $10°\leq\beta\leq 90°$.

We have examined these x-ray sources and find them to contribute negligibly to the total cross section, except in the lower half of the energy range with C, O, and F projectiles on Ni, where they can contribute at most 20%. These corrections were included in the tabulated cross sections to maintain a relative uncertainty of ±1.5% for all the data. The absolute yields in this energy range are uncertain by ±20%. Other contributions, such as x rays produced by δ rays in the target, were not considered.

D. Results

The measured K-shell x-ray yields of $_{13}$Al and $_{28}$Ni for $1\leq Z_1\leq 3$, and the resulting x-ray production cross sections σ_x are listed in Table I. The data for $Z_1=1$ and 2 link up with earlier work[1,20-22] at lower velocities as shown on the semilogarithmic plot in Fig. 5 for Al, and extend beyond the cross section maximum. For later discussion, the reduced Al K-shell ionization cross sections $\sigma_K/Z_1^2=\sigma_x/Z_1^2\gamma_K$ for $1\leq Z_1\leq 3$ are plotted on a linear scale in Fig. 6. The thick-target proton data from KI (open circles) agree within their uncertainties of ±20% with the present thin-target data (solid points) that have relative uncertainties of ±2%. The systematic differences between the data for $Z=1$, 2, and 3 (solid symbols), connected by curves to aid the eye, are significant and well outside experimental uncertainties.

This is brought even more clearly into focus by

TABLE I. Experimental $_{13}$Al and $_{28}$Ni K-shell x-ray production cross sections, σ_x in barns (1 b = 10^{-24} cm^2), for ions of $^1_1$H, $^2_1$H, $^4_2$He, $^6_3$Li, and $^7_3$Li of kinetic energies per mass E_1/M_1, calculated from the measured x-ray yield per target surface density Y/ρ. Uncertainties in percent pertain to the absolute values. Uncertainties of the relative cross sections are ±1.5%. Numbers in parentheses indicate powers of 10. K-shell ionization cross sections are $\sigma_K = \gamma_K^{-1}\sigma_x$, where[18] γ_K(Al) = 0.038 and γ_K(Ni) = 0.41 [note the comment following Eq. (A11)].

		Aluminum (Z_2=13)		Nickel (Z_2= 28)	
		Y/ρ		Y/ρ	
Projectile	E_1/M_1 (MeV/amu) ±0.5%	$\left(\frac{\text{x rays}}{\text{particle}}/\frac{\mu\text{g}}{\text{cm}^2}\right)$ ±3%	σ_x (b) ±10%	$\left(\frac{\text{x rays}}{\text{particle}}/\frac{\mu\text{g}}{\text{cm}^2}\right)$ ±3%	σ_x (b) ±10%
$^1_1$H	2.5	2.13(−5)	9.55(2)	7.76(−7)	7.55(1)
	3.0	2.21(−5)	9.88(2)	1.08(−6)	1.05(2)
	5.0	2.05(−5)	9.16(2)	2.18(−6)	2.12(2)
	7.5	1.74(−5)	7.80(2)	7.80(−6)	3.07(2)
	9.0	1.61(−5)	7.19(2)	3.53(−6)	3.43(2)
	9.75	1.53(−5)	6.83(2)	3.56(−6)	3.48(2)
$^2_1$H	1.0	1.13(−5)	5.04(2)	8.60(−8)	8.37(0)
	1.5	1.69(−5)	7.59(2)	2.63(−7)	2.55(1)
	2.0	1.99(−5)	8.89(2)	5.04(−7)	4.91(1)
	2.5	2.11(−5)	9.46(2)	7.91(−7)	7.70(2)
	3.0	2.18(−5)	9.79(2)	1.10(−6)	1.07(2)
	4.0	2.12(−5)	9.51(2)	1.68(−6)	1.64(2)
	5.0	2.03(−5)	9.07(2)	2.22(−6)	2.16(2)
	6.0	1.89(−5)	8.46(2)	2.65(−6)	2.58(2)
	7.0	1.80(−5)	8.08(2)	3.04(−6)	2.96(2)
	7.5	1.73(−5)	7.75(2)	3.17(−6)	3.08(2)
	9.0	1.58(−5)	7.06(2)	3.47(−6)	3.37(2)
	9.75	1.53(−5)	6.83(2)	3.62(−6)	3.53(2)
$^4_2$He	1.0	4.84(−5)	2.17(3)	2.49(−7)	2.43(1)
	1.5	7.37(−5)	3.30(3)	8.35(−7)	8.13(1)
	2.0	8.74(−5)	3.91(3)	1.84(−6)	1.78(2)
	2.5	9.23(−5)	4.15(3)	2.89(−6)	2.82(2)
	3.0	9.56(−5)	4.28(3)	4.22(−6)	4.11(2)
	4.0	9.20(−5)	4.12(3)	6.78(−6)	6.16(2)
	5.0	8.78(−5)	3.93(3)	9.01(−6)	8.77(2)
	6.0	8.00(−5)	3.58(3)	1.10(−5)	1.08(3)
	7.0	7.56(−5)	3.38(3)	1.29(−5)	1.25(3)
	7.5	7.37(−5)	3.30(3)	1.33(−5)	1.30(3)
$^6_3$Li	3.0	2.39(−4)	1.07(4)	9.15(−6)	8.91(2)
	5.0	3.10(−4)	9.41(3)	2.04(−5)	1.98(3)
	6.0	1.96(−4)	8.80(3)	2.57(−5)	2.51(3)
$^7_3$Li	1.0	1.28(−4)	5.75(3)	4.18(−7)	4.06(1)
	1.5	1.98(−4)	8.85(3)	1.58(−6)	1.54(2)
	2.0			3.56(−6)	3.48(2)
	2.5	2.40(−4)	1.07(4)	6.06(−6)	5.91(2)
	3.0	2.38(−4)	1.06(4)	9.02(−6)	8.79(2)
	4.0	2.26(−4)	1.01(4)	1.50(−5)	1.46(3)
	5.0			2.09(−5)	2.03(3)

the ratios R_{2K} of reduced ionization cross sections measured with two types of projectiles, with charge numbers Z_1 and $Z_1' \geq Z_1$, and masses M_1 and $M_1' \geq M_1$,

$$R_{2K} = \frac{\sigma_K(Z_1')/Z_1'^2}{\sigma_K(Z_1)/Z_1^2} = \frac{\sigma_x(Z_1')/Z_1'^2\gamma_K'}{\sigma_x(Z_1)/Z_1^2\gamma_K} \quad . \tag{21}$$

Table II lists such ratios for $\gamma_K = \gamma_K'$, with uncertainties ±3%, the cross sections ranging in magnitude over a factor of 2 (cf. Fig. 5). For isotopes $Z_1 = Z_1'$ and $M_1' > M_1$, R_{2K} is equal to unity, as predicted for this velocity range where the effect of projectile Coulomb deflection by the target nucleus is negligible. This verifies our experi-

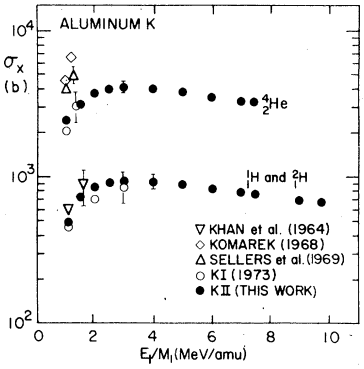

FIG. 5. Al(K) x-ray production cross sections listed in Table I (K II) and earlier measurements (Refs. 1, 20–22).

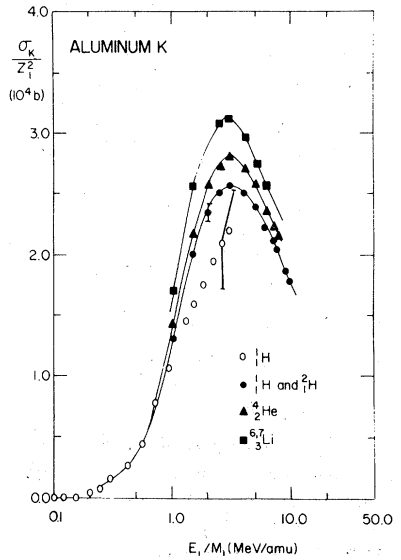

FIG. 6. Linear plot of $_{13}$Al(K) ionization cross sections, with ±2% uncertainty, for $^1_1$H, $^2_1$H, $^4_2$He, and $^{6,7}_3$Li projectiles vs $E_1/M_1 \propto v_1^2$. The open-circle $^1_1$H data, with ±20% uncertainty, are deduced in KI from thick-target yields. The curves, drawn to aid the eye, emphasize the significantly higher σ_K/Z_1^2 values for higher Z_1 projectiles in the E_1/M_1 range 1–10 MeV/amu.

mental procedure and the quoted relative uncertainties. The Al(K) and Ni(K) ratios for $Z_1 = 1$, 2, and 3 are plotted in Figs. 7 and 8.

Table III collates experimental σ_x values of $_{28}$Ni(K) for $^{12}_6$C, $^{16}_8$O, and $^{19}_9$F projectiles. We estimate the absolute values to be uncertain by ±20% when $E_1/M_1 < 0.5$ MeV/amu. With the quoted fluorescence yields, we extract the ionization cross-section ratios shown in Fig. 9.

TABLE II. Ratios R_{2K} of experimental K-shell x-ray production cross sections σ_x as defined by Eq. (21) with $\gamma_K' = \gamma_K$, of $_{13}$Al and $_{28}$Ni for different projectile combinations. Experimental uncertainty is ±2%.

		R_{2K}				
Target	E_1/M_1 (MeV/amu)	$\frac{\sigma_x(^2_1\text{H})}{\sigma_x(^1_1\text{H})}$	$\frac{\sigma_x(^7_3\text{Li})}{\sigma_x(^6_3\text{Li})}$	$\frac{\sigma_x(^4_2\text{He})}{4\sigma_x(^2_1\text{H})}$	$\frac{\sigma_x(^7_3\text{Li})}{9\sigma_x(^2_1\text{H})}$	$\frac{4\sigma_x(^7_3\text{Li})}{9\sigma_x(^4_2\text{He})}$
$_{13}$Al	1.0			1.08	1.26	1.18
	1.5			1.09	1.30	1.20
	2.0			1.10	1.25	
	2.5	0.99		1.10	1.23	1.15
	3.0	0.99	0.99	1.09	1.20	1.11
	4.0			1.08	1.18	1.09
	5.0			1.08	1.15	1.06
	6.0			1.06	1.16	1.09
	7.0			1.05		
	7.5	0.99		1.04		
	9.0	0.99				
	9.5	1.00				
$_{28}$Ni	1.0			0.73	0.54	0.74
	1.5			0.80	0.67	0.84
	2.0			0.91	0.79	0.87
	2.5	1.02		0.92	0.85	0.93
	3.0	1.02	0.99	0.96	0.91	0.95
	4.0			0.94	0.99	1.05
	5.0	1.02	1.03	1.02	1.05	1.05
	6.0			1.05	1.08	1.03
	7.0			1.06		
	7.5	1.00				
	9.0	0.98				
	9.75	1.01				

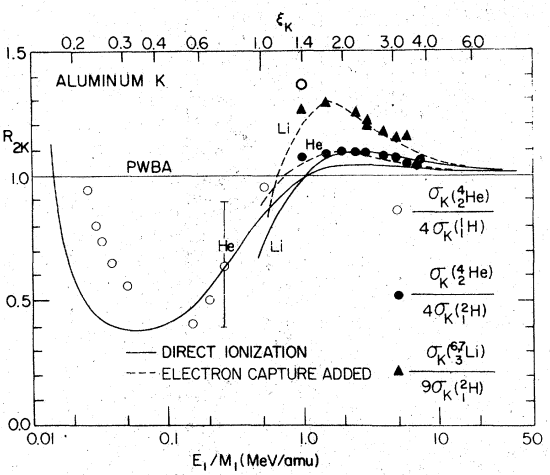

FIG. 7. Cross-section ratios R_{2K}, Eq. (21), for $_{13}$Al(K) ionization by four different projectiles with $Z_1 \leq 3$, as a function of E_1/M_1 and ξ_K, Eq. (1). The open symbols with ± 35% uncertainty are deduced in KI from thick-target x-ray yields. The line at 1 is the PWBA prediction. The solid curves labeled He and Li predicted by Eq. (47) for direct ionization with Coulomb deflection, binding, and polarization effects. The dashed curves include electron capture by the projectiles.

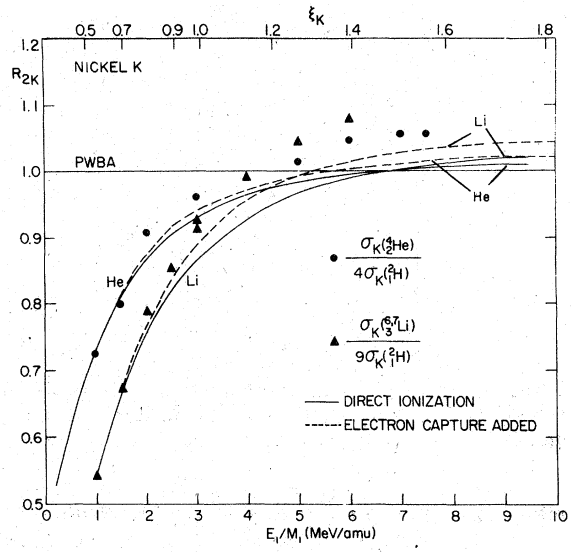

FIG. 8. Same as Fig. 7 for Ni(K) ionization cross sections, with Z_1=1, 2, and 3.

III. THEORY

As delineated in KI, one can describe an ionizing collision between a charged particle and an atom with the Hamiltonian

$$H = H_0 + gH_1 + hV_0 , \tag{22}$$

where H_0 refers to the noninteracting particle-atom system, gH_1 to the deflecting Coulomb interaction of strength g between the particle and the atomic nucleus, and hV_0 to the ionizing Coulomb interaction of strength h. According to KI, gH_1 can be neglected in velocity regime II. In the semiclassical approximation (SCA) this is equivalent to describing projectile trajectories as straight lines.

The calculations consider transitions of the electron from the target K shell to the continuum called "direct ionizations" in distinction to K-shell vacancy formation through electron capture (EC) by the projectile when $Z_1 > 1$. Electron capture into bound projectile states[23] increases the total ionization cross section.

The development of the Coulomb-ionization cross section,

$$\sigma = h^2 T_2 + h^3 T_3 + \cdots , \tag{23}$$

gives as the first term the plane-wave Born-approximation cross section σ^{PWBA}. The second term accounts to lowest order for the perturbation of the target atom by the projectile and, specifically, when $h = Z_1/Z_2$, gives rise to Z_1^3 proportional polarization effects.[3] *In regime I*, ionization occurs in deep, slow collisions, and Coulomb deflection and changes in the K-shell binding energies give rise to *subtractive effects* which *decrease* the cross sections.[1] *In regime II*, collisions with impact parameters comparable to and larger than the K-shell radius contribute, and the attendant polarization of the shell by the projectile gives rise to *additive effects* which *increase* the cross sections. Guided by the PSS formalism we derive the high-velocity polarization effect along the lines developed for stopping

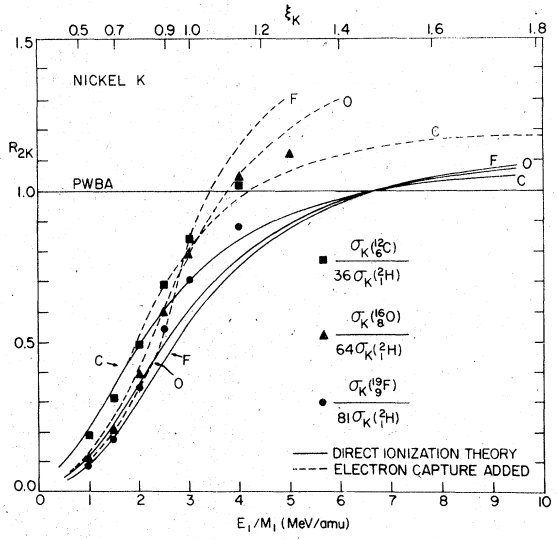

FIG. 9. Same as Figs. 7 and 8 for Ni(K) ionization cross sections, with Z_1=6, 8, and 9.

TABLE III. Experimental $_{28}$Ni K-shell x-ray production cross sections σ_x and ionization cross sections $\sigma_K = \bar{\gamma}_K^{-1}\sigma_x$ for ions of $^{12}_{6}$C, $^{16}_{8}$O, and $^{19}_{9}$F, with kinetic energies per mass E_1/M_1 calculated from measured x-ray yields per target surface density Y/ρ and corrected at the lowest energy (by less than 20%) for secondary target effects as described by Eqs. (16)–(20). The effective fluorescence yield $\bar{\gamma}_K$ changes relative to[18] $\gamma_K = 0.41$ are tabulated below and shown in Fig. 3. Uncertainties of absolute values are ±20% for $E_1/M_1 < 0.5$ MeV/amu, and ±10% for $E_1/M_1 > 0.5$ MeV/amu. Uncertainties of the relative cross sections are ±1.5%. Numbers in parentheses indicate powers of 10.

			Nickel ($Z_2 = 28$)		
Projectile	E_1/M_1 (MeV/amu)	Y/ρ $\left(\frac{\text{x rays}}{\text{particle}}/\frac{\mu\text{g}}{\text{cm}^2}\right)$	σ_x (b)	$\bar{\gamma}_K/\gamma_K$ ($\gamma_K = 0.41$)	σ_K (b)
$^{12}_{6}$C	0.375	1.22(−8)	1.20(0)	1.00	2.92(0)
	0.50	4.71(−8)	4.58(0)	1.00	1.12(1)
	0.75	1.52(−7)	1.59(1)	1.03	3.79(1)
	1.0	6.16(−7)	6.01(1)	1.07	1.40(2)
	1.25	1.60(−6)	1.55(2)	1.09	3.55(2)
	1.50	3.22(−6)	3.14(2)	1.09	7.05(2)
	1.75	6.48(−6)	6.31(2)	1.09	1.41(3)
	2.0	9.76(−6)	9.51(2)	1.10	2.11(3)
	2.5	2.15(−5)	2.02(3)	1.09	4.66(3)
	3.0	3.61(−5)	3.52(3)	1.09	7.90(3)
	3.5	5.18(−5)	5.05(3)	1.08	1.15(4)
	4.0	6.63(−5)	6.45(3)	1.08	1.47(4)
	4.5	8.56(−5)	8.34(3)	1.07	1.90(4)
$^{16}_{8}$O	0.375	1.50(−8)	1.46(0)	1.00	3.56(0)
	0.50	3.65(−8)	3.54(0)	1.00	8.64(0)
	0.75	2.08(−7)	2.02(1)	1.05	4.69(1)
	1.0	6.53(−7)	6.35(1)	1.08	1.43(2)
	1.5	3.89(−6)	3.80(2)	1.13	8.24(2)
	2.0	1.43(−5)	1.39(3)	1.14	2.97(3)
	2.5	3.45(−5)	3.36(3)	1.14	7.17(3)
	3.0	6.34(−5)	6.17(3)	1.14	1.32(4)
	3.5	8.52(−5)	8.30(3)	1.13	1.80(4)
	4.0	1.26(−4)	1.24(4)	1.13	2.68(4)
	4.5	1.53(−4)	1.49(4)	1.12	3.26(4)
	5.0	1.76(−4)	1.72(4)	1.11	3.78(4)
	5.7	2.38(−4)	2.31(4)	1.10	5.12(4)
$^{19}_{9}$F	0.375	1.24(−8)	1.21(0)	1.00	2.95(0)
	0.50	3.45(−8)	1.07(0)	1.00	8.21(0)
	0.75	2.25(−7)	2.19(1)	1.08	4.57(1)
	1.0	6.34(−7)	6.17(1)	1.15	1.30(2)
	1.5	4.33(−6)	4.23(2)	1.18	8.78(2)
	2.0	1.66(−5)	1.62(3)	1.18	3.35(3)
	2.5	4.14(−5)	4.04(3)	1.18	8.34(3)
	3.0	7.33(−5)	7.13(3)	1.17	1.48(4)
	3.5	1.13(−4)	1.10(4)	1.16	2.30(4)
	4.0	1.55(−4)	1.50(4)	1.15	2.86(4)
	4.5	2.17(−4)	2.11(4)	1.14	4.53(4)

powers, and construct the transition between the binding and polarization effects in the intermediate velocity regime II.

A. Polarization effects

Following the first formulation[3] we write Eq. (23) in the form

$$\sigma_K = \sigma_K^{\mathrm{PWBA}} + 2\int d\omega\, s_K(\omega)\left(2\pi\int_0^\infty P_3(\omega,b)\, b\, db\right) + O(Z_1^4)\,, \tag{24}$$

where

$$\sigma_K^{\mathrm{PWBA}} = 4\pi\int_0^\infty b\, db \int_{\omega_{2K}}^\infty p(\omega,b)d\omega\,,$$

in terms of the differential ionization probability per electron, $p(\omega,b)$, which is proportional to Z_1^2. This formula embodies the identity of the cross section in the PWBA and the SCA.[24] In K shells, most collision-induced transitions reach into the continuum, and one can identify $s_K(\omega)$ with the K-shell differential oscillator-strength distribution per electron, as the leading factor of 2 implies. The function $P_3(\omega,b)$ is an effective probability, proportional to Z_1^3, for an energy transfer $\hbar\omega$ to an initial state that is perturbed by the projectile moving on a trajectory with impact parameter b.

In deriving P_3, we follow the quantum-mechanical development of the polarization effect for a harmonic oscillator by Hill and Merzbacher,[25] and apply it to the atomic K shell through the oscillator strength. The treatment starts with the large impact-parameter parts of a multipole expansion of the ionizing Coulomb-interaction potential and retains the dominant dipole and quadrupole terms. The transition probability for an energy transfer ΔE appears as a series, where the leading term P_2 comes from the dipole interaction only and is proportional to Z_1^2 as in the plane-wave Born approximation. The next contribution P_3 stems from the interference between the dipole and quadrupole terms in the transition-amplitude expansion and is proportional to Z_1^3. We identify $\Delta E = \hbar\omega(P_2+P_3)$ in Eq. (32) of Ref. 25 and cull the expression

$$P_3(b,\omega)=\frac{2(Z_1e^2)^3}{\hbar\omega m^2v_1^4b^3}\left(-K_1(u)\int_{-\infty}^{+\infty}\frac{dv\cos(uv)}{(1+v^2)^{5/2}}[(v^2-2)F_1(u,v)-3vF_2(u,v)]\right.$$
$$\left.+K_0(u)\int_{-\infty}^{+\infty}\frac{dv\sin(uv)}{(1+v^2)^{5/2}}[3vF_1(u,v)-(1-2v^2)F_2(u,v)]\right)\Theta(b-a_\omega), \tag{25}$$

where a_ω is a constant, $u\equiv\omega b/v_1$,

$$F_1(u,v)=\int_{-\infty}^{v}\frac{dy\sin[u(v-y)]}{(1+y^2)^{3/2}},$$

and

$$F_2(u,v)=\int_{-\infty}^{v}\frac{dyy\sin[u(v-y)]}{(1+y^2)^{3/2}}.$$

The step function $\Theta(b-a_\omega)$ limits the contributions to impact parameters larger than a_ω. Integration over impact parameters as prescribed by Eq. (24) yields

$$2\pi\int_0^\infty P_3(b,\omega)b\,db=\frac{4\pi(Z_1e^2)^3}{\hbar m^2v_1^5}I\left(\frac{\omega a_\omega}{v_1}\right). \tag{26}$$

The polarization function $I(x)$ was first derived starting from a classical harmonic-oscillator model.[8] Numerical values of $I(x)$ are given in Table IV.[26] A suitable interpolation formula, with error less than 1%, is

$$I(x)=\begin{cases}\frac{3}{4}\pi\left(\ln\frac{1}{x^2}-1\right) & \text{for } 0<x\leq 0.035,\\ e^{-2x}(0.031+0.210x^{1/2}+0.005x & \\ \quad -0.069x^{3/2}+0.324x^2)^{-1} & \\ & \text{for } 0.035<x\leq 3.1.\end{cases} \tag{27}$$

When $x>3.1$, $I(x)<7\times10^{-4}$ and can be neglected in practice.

At high velocities, I depends on the model-dependent parameter a_w only logarithmically and may be adjusted to fit experimental data.[8] This constant represents the small-impact-parameter limit below which the energy transfer becomes so large that the

TABLE IV. Selected values of the polarization function $I(x)$ introduced in Eq. (26) and appearing in Eq. (46).[26] Numbers in parentheses indicate powers of 10. Interpolations according to Eq. (27).

x	$I(x)$	x	$I(x)$	x	$I(x)$	x	$I(x)$
1.0(−3)	3.01(1)	2.0(−1)	5.02(0)	3.5(0)	2.40(−4)	8.0(0)	7.73(−9)
2.0(−3)	2.68(1)	3.0(−1)	3.29(0)	4.0(0)	7.58(−5)	8.5(0)	2.70(−9)
5.0(−3)	2.25(1)	5.0(−1)	1.53(0)	4.5(0)	2.28(−5)	9.0(0)	9.10(−10)
1.0(−2)	1.93(1)	8.0(−1)	5.32(−1)	5.0(0)	7.01(−6)	9.5(0)	3.08(−10)
2.0(−2)	1.60(1)	1.0(0)	2.72(−1)	5.5(0)	2.20(−6)	1.0(1)	1.05(−10)
3.0(−2)	1.41(1)	1.5(0)	5.72(−2)	6.0(0)	7.01(−7)	1.1(1)	1.25(−11)
5.0(−2)	1.16(1)	2.0(0)	1.27(−2)	6.5(0)	2.26(−7)	1.2(1)	1.79(−12)
8.0(−2)	9.35(0)	2.5(0)	3.13(−3)	7.0(0)	7.36(−8)	1.3(1)	2.25(−13)
1.0(−1)	8.27(0)	3.0(0)	8.37(−4)	7.5(0)	2.40(−8)	1.4(1)	2.65(−14)

initial state binding energy can be neglected. Under these conditions the collision is described by pure Rutherford scattering which is proportional to Z_1^2. Setting a_ω equal to the harmonic-oscillator radius[27] $a_\omega=(\hbar/2m\omega)^{1/2}$, one has $I(\omega a_\omega/v_1)=I[(\hbar\omega/2mv_1^2)^{1/2}]$. Recent stopping-power data[28] support a smaller value of a_ω, perhaps close to that suggested by other models,[29] $a_\omega=\hbar/\gamma mv_1$, where γ is Euler's constant, whence $I(\omega a_\omega/v_1)\simeq I(\hbar\omega/2mv_1^2)$. With these arguments, the high-velocity limit $v_1\gg\omega a_\omega$ of $I(x)$ takes the simple form

$$I=\frac{3\pi}{4}\left[G\ln\left(\frac{2mv_1^2}{\hbar\omega}\right)-1\right], \tag{28}$$

with the appearance of the stopping number $\ln(2mv_1^2/\hbar\omega)$ of the Bethe stopping-power formula. The constant G, of value 1 if $a_\omega=(\hbar/2m\omega)^{1/2}$ or 2 if $a_\omega=\hbar/2mv_1$, is a reminder of the model dependence of a_ω. Equation (26) becomes

$$2\pi\int_0^\infty P_3(b,\omega)b\,db=\frac{3\pi^2(Z_1e^2)^3}{\hbar m^2v_1^5}\left[G\ln\left(\frac{2mv_1^2}{\hbar\omega}\right)-1\right]. \tag{29}$$

We represent the differential oscillator strength $s_K(\omega)$ as a power law,[30]

$$s_K(\omega)=l\omega_{2K}^l/\omega^{l+1}, \tag{30}$$

normalized as

$$\int_{\omega_{2K}}^\infty s_K(\omega)d\omega=1.$$

The parameter value $l=\frac{5}{3}$ provides a good fit to the K-shell oscillator-strength distribution. Integration of Eq. (24) gives

$$\sigma_K=\sigma_K^{\mathrm{PWBA}}+\frac{6\pi^2(Z_1e^2)^3}{\hbar m^2v_1^5}\left[G\ln\left(\frac{2mv_1^2}{\hbar\omega_{2K}}\right)-1-\frac{G}{l}\right], \tag{31}$$

or, in terms of the reduced variable ξ_K, Eq. (1),

$$\sigma_K(\xi_K;\Theta_K)=\sigma_K^{\mathrm{PWBA}}(\xi_K;\Theta_K)+6\pi^2a_{2K}^2\left(\frac{Z_1}{Z_{2K}}\right)^3\times\left(\frac{2}{\Theta_K\xi_K}\right)^5\left(G\ln(\Theta_K\xi_K^2)-1-\frac{G}{l}\right). \tag{32}$$

The additive polarization term in this expression is valid in the range $\xi_K\gg1$ of regime III. As ξ_K approaches unity from above, the polarization effect contributes significantly to σ_K,[3] but the theory underlying Eq. (31) becomes inadequate. Interpolation schemes must be devised to build a link in the intermediate range $\xi_K\simeq1$ to the low-velocity binding effect derived in KI for $\xi_K\ll1$.

B. Intermediate-velocity regime

We proceed by developing an effective binding energy $\hbar\omega_{2K}'$ for the electrons to be excited. At low-particle velocities ω_{2K}' is enhanced over ω_{2K} by $\Delta\omega_{2K}(b)$, which accounts for the binding effect.[4,31] The high-velocity polarization effect causes an increase in the energy transfer that is treated in what follows as a reduction in the binding energy. We extend Eq. (24) as

$$\sigma_K=4\pi\int_0^\infty b\,db\int_{\omega_{2K}+\Delta\omega_{2K}(b)}^\infty p(\omega,b)d\omega+4\pi\int_0^\infty b\,db\int_{\omega_{2K}}^\infty s_K(\omega)P_3(\omega,b)d\omega. \tag{33}$$

The low-velocity binding effect, introduced through the lower-integration limit as $\Delta\omega_{2K}(b)$, is discussed in detail in Appendix A for KI [cf. Eq. (A4)], and substantiated in the perturbed-stationary state theory.[4] We extend this approach to higher velocities and define a v_1-dependent function ζ_K so that

$$\sigma_K=4\pi\int_{\zeta_K\omega_{2K}}^\infty d\omega\int_0^\infty b\,db\,p(\omega,b) \tag{34}$$

accounts for binding effects in regime I and polarization effects in regimes II and III.

Expanding Eq. (34) in a Taylor series about ω_{2K} gives, to first order in (ζ_K-1),

$$\sigma_K=\sigma_K^{\mathrm{PWBA}}-4\pi\int_0^\infty b\,db\,p(\omega_{2K},b)(\zeta_K-1)\omega_{2K}, \tag{35}$$

while the analogous expansion of the first term in Eq. (33) yields

$$\sigma_K=\sigma_K^{\mathrm{PWBA}}-4\pi\int_0^\infty b\,db\left(p(\omega_{2K},b)\Delta\omega_K(b)-\int_{\omega_{2K}}^\infty d\omega\,s_K(\omega)P_3(\omega,b)\right). \tag{36}$$

We interpolate by limiting binding effects to $b\leq c_Ka_{2K}$ and polarization effects to $b\geq c_K'a_{2K}$, where c_K and c_K' are constants of order unity.[3] By equating Eqs. (35) and (36) and solving, we obtain

$$\zeta_K(\xi_K)=\epsilon_K(\xi_K,c_K)-\frac{\int_{c_K'a_{2K}}^\infty b\,db\int_{\omega_{2K}}^\infty d\omega\,s_K(\omega)P_3(\omega,b)}{\omega_{2K}\int_0^\infty b\,db\,p(\omega_{2K},b)}, \tag{37}$$

where

$$\epsilon_K(\xi_K,c_K)=1+\frac{\int_0^{c_Ka_{2K}}b\,db\,p(\omega_{2K},b)\Delta\omega_K(b)}{\omega_{2K}\int_0^\infty b\,db\,p(\omega_{2K},b)}=1+\frac{2}{\Theta_K}\frac{Z_1}{Z_{2K}}g(\xi_K,c_K). \tag{38}$$

The probability $p(\omega_{2k}, b)$ is proportional to $(b\omega_{2K}/v_1)^4 K_2^2(b\omega_{2K}/v_1)$ in the low-velocity limiting form, KI Eq. (A1), to which only s waves ($l=0$) in the electron continuum contribute; it can be approximated[2] as $x^4K_2^2(x) = (\frac{1}{2}\pi x^3 + 6x^2 + 8x + 4)e^{-2x}$, where K_2 is the modified Bessel function of the second kind. All partial waves are included in the cross sections. The contributions of $l>0$ waves at intermediate velocities are decisive. But their contribution to the waning energy shift giving the binding effect on the cross sections at these velocities is small and does not warrant a complete partial-wave calculation of the shift at this stage of development of the theory. We use the low-velocity expression for $p(\omega_{2K}, b)$ to calculate the shift at intermediate velocites. This gives the advantage of an analytical form, while compensating in an average manner for the omission of the $l>0$ contributions to the energy shift by a commensurate overestimate of the $l=0$ contribution in this velocity range. The calculation of the function $g(\xi_K, c_K)$ according to Eq. (A13) of KI is straightforward, but lengthy, and yields the result

$$g_K(\xi_K, c_K) = \frac{8}{\xi_K(3\pi+42)}\,(f_0 - f_1 e^{-2x} + f_2 e^{-2y}), \tag{39}$$

where $x \equiv c_K/\xi_K$, $y \equiv c_K + x$, and

$$f_0 = \frac{3\pi+88}{16} - \frac{3}{8}\,\frac{6\xi_K + \frac{1}{2}\pi + \pi\xi_K/(1+\xi_K)}{(1+\xi_K)^4} - \frac{1}{4}\,\frac{8\xi_K+6}{(1+\xi_K)^3} - \frac{3\xi_K+4}{(1+\xi_K)^2}, \tag{40}$$

$$f_1 = \tfrac{11}{2} + \tfrac{3}{16}\,\pi + \tfrac{1}{4}\,\pi x^3 + 3\,(1+\tfrac{1}{8}\,\pi)x^2 + (7+\tfrac{3}{8}\,\pi)x, \tag{41}$$

$$f_2 = \frac{2}{1+\xi_K} + \frac{(2+\xi_K)(1+2y)}{(1+\xi_K)^2} + \frac{4y^3+6(1+y)y+3}{(1+y)^5} \times [\tfrac{1}{16}\,\pi + (\tfrac{3}{4} + \tfrac{3}{16}\,\pi)\xi_K + \tfrac{3}{4}\,\xi_K^2] + \frac{\pi\xi_K x^4}{4(1+\xi_K)} + \frac{4\xi_K+3}{2(1+\xi_K)^3}\,(1+2y+2y^2). \tag{42}$$

Selected values of g_K are listed in Table V. Equation (39) reduces to Eq. (39) of KI for $c_K \to \infty$.

Since P_3 is a slowly varying function of ω compared to $s_K(\omega)$, we calculate the numerator of the second term in Eq. (37) as

$$\int_{c_K' a_{2K}}^{\infty} b\,db \int_{\omega_{2K}}^{\infty} d\omega\, s_K(\omega) P_3(\omega, b) \simeq 2a_{2K}^2 \left(\frac{Z_1}{Z_{2K}}\right)^3 \left(\frac{2}{\Theta_K \xi_K}\right)^5 I\left(\frac{c_K'}{\xi_K}\right), \tag{43}$$

and relate the integral in the denominator to

$$4\pi \int_0^{\infty} b\,db\, p(\omega_{2K}, b) = \left(\frac{d\sigma_K^{\mathrm{PWBA}}}{d\omega}\right)_{\omega=\omega_{2K}} = 8\pi a_{2K}^2 \left(\frac{Z_1}{Z_{2K}}\right)^2 \left(\frac{2}{\Theta_K \xi_K}\right)^2 \times s_K(\Theta_K) L(\xi_K, \Theta_K), \tag{44}$$

where $s_K(\Theta_K)\,L(\xi_K, \Theta_K)$ is the tabulated K-shell excitation function,[6] with the asymptotic form of $L = \ln(\frac{1}{2}\Theta_K \xi_K)^2 + \text{const} = \ln\eta_K + \text{const}$. In the ξ_K range of interest for the polarization effect, we treat $\Theta_K L$ as a constant, with an appropriate mean value of $\frac{6}{5}$.

The choice of c_K and c_K' is a delicate problem. For definiteness, we set $c_K = c_K'$. This assumes that projectiles with impact parameter $< c_K a_{2K}$ cause the binding effect, while the remaining particles produce the polarization effect. Equation (37) becomes

$$\zeta_K(\xi_K, c_K) = 1 + \frac{2}{\Theta_K}\,\frac{Z_1}{Z_{2K}}\,[g(\xi_K, c_K) - h(\xi_K, c_K)], \tag{45}$$

where $g(\xi_K, c_K)$ can be gleaned from Eqs. (39)–(42), and

$$h(\xi_K, c_K) = (2/\Theta_K \xi_K^3)\, I(c_K/\xi_K). \tag{46}$$

Given $\zeta_K(\xi_K, c_K)$, where ξ_K is defined in Eq. (1), the ionization cross section for nonrelativistic K-shell electrons and particle velocities can be written in a comprehensive manner as

$$\sigma_K = C_K(\pi\, dq_0 \zeta_K)\sigma_K^{\mathrm{PWBA}}(\eta_K; \zeta_K\Theta_K) \simeq C_K(\pi\, dq_0 \zeta_K)\,\frac{\sigma_{0K}}{\zeta_K \Theta_K} F_K\left(\frac{\eta_K}{(\xi_K\Theta_K)^2}\right) \tag{47}$$

in terms of the particle velocity parameter η_K, Eqs. (2) or (3), and the constant $\sigma_{0K} = 8\pi a_{2K}^2 (Z_1/Z_{2K})^2$. The function $F_K(y)$ is tabulated in KI and can be calculated accurately by the formula $F_K(y) = (2^{17}/45)y^4/(1+6.88\,y)^4$ for $y \leq 0.05$.

The Coulomb deflection factor $C_K(x)$ depends through $x \equiv \pi\, dq_0 \zeta_K$ on $q_0 = \omega_{2K}/v_1$ and the half-distance of closest approach, d, in a head-on collision between the nuclei of the projectile (Z_1, M_1) and the target atom (Z_2, M_2); $d = Z_1 Z_2 e^2/Mv_1^2$ with $M = (M_1^{-1} + M_2^{-1})^{-1}$. As derived in Ref. 3,

$$C_K(x) = 9\int_1^{\infty} t^{-10} C(xt)\, dt. \tag{48}$$

If the differential Coulomb deflection function, $C(y)$, is given by $C(y) = \exp(-y)$, one obtains[3]

$$C_K(x) = 9\int_1^{\infty} t^{-10} e^{-xt}\, dt \equiv 9E_{10}(x). \tag{49}$$

Recent calculations[32,33] suggest that $C(y)$ declines

TABLE V. The function $g(\xi_K, c_K)$ as given by Eqs. (39)–(42). The last column, for $c_K = 100$, coincides with the function $g(\xi_K)$ tabulated in KI, Table VI, which is valid for $c_K \to \infty$.

	$g(\xi_K, c_K)$							
ξ_K	$c_K=0.5$	0.75	1.0	1.5	2.0	5.0	10	100
0.00	1.000	1.000	1.000	1.000	1.000	1.000	1.000	1.000
0.04	0.996	0.996	0.996	0.996	0.996	0.996	0.996	0.996
0.08	0.984	0.985	0.985	0.985	0.985	0.985	0.985	0.985
0.16	0.859	0.941	0.951	0.953	0.953	0.953	0.953	0.953
0.24	0.641	0.829	0.891	0.911	0.912	0.912	0.912	0.912
0.32	0.462	0.683	0.796	0.860	0.868	0.869	0.869	0.869
0.40	0.339	0.549	0.687	0.799	0.821	0.826	0.826	0.826
0.48	0.256	0.441	0.583	0.729	0.771	0.784	0.784	0.784
0.56	0.198	0.357	0.493	0.656	0.718	0.745	0.745	0.745
0.64	0.157	0.292	0.417	0.587	0.664	0.708	0.708	0.709
0.72	0.127	0.243	0.355	0.523	0.611	0.674	0.674	0.674
0.80	0.105	0.204	0.304	0.465	0.560	0.642	0.643	0.643
0.88	0.088	0.173	0.263	0.415	0.512	0.613	0.613	0.614
0.96	0.075	0.149	0.229	0.371	0.468	0.585	0.586	0.587
1.00	0.069	0.139	0.214	0.351	0.447	0.572	0.574	0.574
1.20	0.049	0.100	0.157	0.269	0.358	0.511	0.517	0.517
1.40	0.036	0.075	0.120	0.211	0.290	0.458	0.469	0.469
1.60	0.028	0.058	0.094	0.169	0.238	0.411	0.429	0.429
1.80	0.022	0.046	0.075	0.138	0.197	0.369	0.395	0.395
2.00	0.018	0.038	0.062	0.115	0.166	0.332	0.365	0.366
2.20	0.015	0.031	0.051	0.096	0.141	0.299	0.339	0.341
2.40	0.013	0.027	0.044	0.082	0.121	0.270	0.316	0.310
2.60	0.011	0.023	0.037	0.071	0.105	0.244	0.295	0.299
2.80	0.009	0.020	0.032	0.062	0.092	0.221	0.276	0.282
3.00	0.008	0.017	0.028	0.054	0.081	0.201	0.259	0.266
3.40	0.006	0.013	0.022	0.043	0.064	0.168	0.228	0.240
3.80	0.005	0.011	0.018	0.034	0.052	0.142	0.203	0.218
4.20	0.004	0.009	0.015	0.028	0.043	0.121	0.181	0.200
4.60	0.003	0.007	0.012	0.024	0.036	0.104	0.162	0.185
5.00	0.003	0.006	0.010	0.020	0.031	0.090	0.145	0.171
6.00	0.002	0.004	0.007	0.014	0.022	0.065	0.113	0.145
7.00	0.001	0.003	0.005	0.010	0.016	0.049	0.089	0.120
8.00	0.001	0.002	0.004	0.008	0.012	0.039	0.072	0.111
9.00	0.001	0.002	0.003	0.006	0.010	0.031	0.059	0.100

faster than exponentially with increasing y such that $C_K(x)$ is smaller than $9E_{10}(x)$ for $x \gtrsim 1$.

To date, experiments extend in x as far as $x = 2.8$. For the largest x in recent data[34] (1.2-MeV α particles on $_{64}$Gd, $x = 2.56$), Eq. (47) with $C_K = 9E_{10}(2.56) = 0.060$ overestimates the ionization cross sections by a factor 4.3 relative to experiment when a correction is made for relativistic K-shell effects (CPSSR) in $_{64}$Gd. Extension of the $C(y)$ calculations in Ref. 32 and integration according to Eq. (48) yields $C_K(2.56) \simeq 0.005$. With this value the theory predicts a cross section that is smaller than the measured one by a factor $\sim\frac{1}{3}$. If this description of the Coulomb deflection effect is correct, then the relativistic K-shell effects in $_{64}$Gd may have been underestimated in Ref. 34 by such a factor.

The results of our theory, although cast in terms of the plane-wave Born approximation with scaled variables, should not be viewed as a "corrected PWBA." Equation (47) owes its genesis to the perturbed stationary state approach, and is the result of a CPSS approximation: the projectiles on classical trajectories are Coulomb deflected (C), and the target atoms are described by perturbed stationary states (PSS) to account for the binding and polarization effects. The CPSS formula applies to the direct ionization by projectiles with $Z_1 \ll Z_2$ at all velocities. Electron capture by the projectile contributes noticeably when $Z_1 > 1$ in the range $1 \lesssim \xi_K \lesssim 5$.

IV. DISCUSSION

We emphasize the new effects incorporated in Eq. (47) by focusing on cross-section ratios R_{2K} Eq. (21) and listed in Table II.

Extensive sample calculations have shown that the magnitude of the binding effect at $\xi_K < 1$ and of

the polarization effect at $\xi_K > 1$ are insensitive to the detailed choice of $c_K \simeq 1$. Merely the value of ξ_K^c at which $\sigma_K/\sigma_K^{\mathrm{PWBA}} = 1$ shifts with c_K to larger values. As a trial value we choose $c_K = \frac{3}{2}$ such that the transition between the binding effect and the polarization effect occurs at impact parameters equal to the expectation value, $\langle r\rangle_{2K} = \frac{3}{2}a_{2K}$, of the radial electron distance in the K shell. The R_{2K} curves for Al, shown in Fig. 7, were calculated for direct ionization from Eqs. (21) and (47). They cross the $R_{2K} = 1$ line at $\xi_K^c = 1.4$. The theory predicts the ratios accurately for $Z_1 \leq 2$, to within 10%, in a range of E_1/M_1 values over which cross sections vary by six orders of magnitude. The data approach unity from above, i.e., the cross sections become strictly proportional to Z_1^2 when $\xi_K \gtrsim 5$.[35] The theoretical ratios are compared with the Ni data in Fig. 8.

Given c_K, the crossing points at $\xi_K = \xi_K^c$ increase linearly with Θ_K. For $c_K = 1.5$, numerical evaluation of the theory predicts crossing points as a function of Θ_K which are fitted by $\xi_K^c = 0.74 + 0.89\,\Theta_K$. Present experimental evidence suggests crossing points at ξ_K values ranging from 1.0 to 1.4.[36-38] The contributions of electron capture by the projectiles to ionization increase R_{2K} at intermediate velocities and lower the observed ξ_K^c values relative to the values predicted from the direct-ionization theory. Examples are shown in Figs. 7 and 8 for projectiles with $Z \leq 3$ in $_{13}$Al and $_{28}$Ni, and in Fig. 9 for the projectiles with $6 \leq Z_1 \leq 9$ in $_{28}$Ni.

One may calculate the cross section σ_K^{EC} for electron capture by a projectile from the target K shell, starting with Eq. (20) of Ref. 23, using a cut off in the binding effect[39] consistent with $c_K = \frac{3}{2}$, and multiplying it by the density of final states, $\mathfrak{N}_f$, on the projectiles. We set the mean number of vacancies on the projectile equal to the number of stripped electrons at v_1, $\mathfrak{N}_f Z_1 \simeq Z_1[1 - \exp(-0.95 v_1/Z_1^{2/3} v_0)]$.[4] In our range of Z_1, Z_2, and v_1, the predictions of Eq. (20) in Ref. 23 with Nikaloev cross sections[41] calculated in the Oppenheimer-Brinkman-Kramers (OBK) approximation with screened hydrogenic wave functions can be approximated to within 30% by the expedient formula[42]

$$\sigma_K^{\mathrm{EC}} = \mathfrak{N}_f \frac{2^{19}\pi a_0^2 (Z_1 Z_{2K})^5 v_1^8}{5\{A v_1^4 + 2B v_1^2 [C(v_1) Z_{2K}^2 + Z_1^2] + [C(v_1) Z_{2K}^2 - Z_1^2]^2\}^5} , \tag{50}$$

with

$$A = 3^{1/5}, \quad B = 2\left(1 - \tfrac{4}{3} Z_1/Z_{2K}\right), \quad C = \Theta_K \left[1 + (2Z_1/\Theta_K Z_{2K}) g_K(\xi_K'; \tfrac{3}{2})\right] .$$

The function g_K is given by Eq. (39) and Table V, and ξ_K is taken to be

$$\xi_K' = \xi_K \Theta_K \{[\Theta_K - (Z_1/Z_{2K})^2 + \eta_K]^2 + 4(Z_1/Z_{2K})^2\}^{-1/2} .$$

The form of Eq. (50) is guided by the hydrogenic OBK approximation and designed, through A and $C(v_1)$, to retain the proper asymptotic behavior at high- and low-projectile velocities; B serves as an interpolation parameter. In terms of σ_{0K} in Eq. (47) and of ξ_K in Eq. (1), or η_K in Eq. (2), Eq. (50) can be written as

$$\sigma_K^{\mathrm{EC}} = \mathfrak{N}_f \left(\frac{Z_1}{Z_{2K}}\right)^3 \sigma_{0K} \frac{2^{16}\eta_K^4}{5\{A\eta_K^2 + 2B\eta_K[C + (Z_1/Z_{2K})^2] + [C - (Z_1/Z_{2K})^2]^2\}^5} . \tag{51}$$

The cross-section ratio R_{2K}' to be compared with experiment becomes

$$R_{2K}' = \frac{[\sigma_K(Z_1') + \sigma_K^{\mathrm{EC}}(Z_1')]/Z_1'^2}{[\sigma_K(Z_1) + \sigma_K^{\mathrm{EC}}(Z_1)]/Z_1^2} . \tag{52}$$

The dashed curves in Figs. 7–9 represent Eq. (52), with σ_K calculated according to Eq. (47) and σ_K^{EC} according to Eq. (51).

As Z_1 approaches Z_2, Pauli excitation through the overlap of target and projectile electron structures during collisions becomes important at low velocities,[43,44] and inner-shell ionizations in such collisions cannot be described as Coulomb excitation. Coulomb excitation dominates at low velocities, $\xi_K < 1$, when $a_{1K} \gg a_{2K}$, i.e., $Z_1/Z_2 \ll 1$. The projectile then acts as a bare charge in the small-impact-parameter collisions which contribute most to the ionization cross section.[1] Coulomb excitation also dominates at intermediate and high velocities $\xi_K \gtrsim 1$, provided the projectile is then stripped of

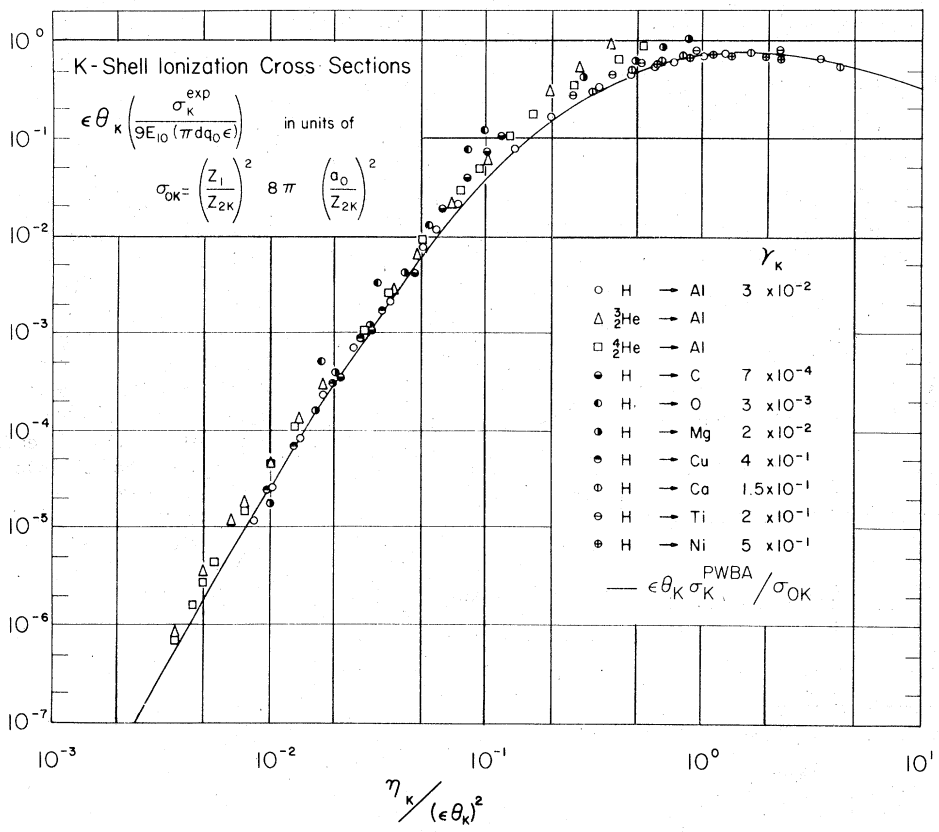

FIG. 10. Universal plot of K-shell ionization cross sections of different targets for $^1_1$H and $^{3,4}_2$He projectiles, in the reduced form given in KI, which does not include polarization effects. The He data are generally higher than the H data.

electrons. This occurs if the projectile moves in the target with velocity $v_1 > Z_1 v_0$. Combining these restrictions implies the sufficient condition $Z_1/Z_2 < \frac{1}{2}\Theta_K$ for Coulomb ionization to dominate at all particle velocities. There is ample evidence that the comprehensive description of Coulomb excitation by bare particles is valid in this range of Z_1/Z_2. If the particles are not fully stripped, the screening of the projectile charge may reduce the cross sections in the intermediate-velocity domain.[45-47]

Detailed spectroscopic K x-ray data have resolved the relative yields from the different vacancy distributions created in other shells with the creation of a K-shell vacancy.[48] We note that the formulae developed in KI and KII apply when the sum is taken over all transitions which create a K-shell vacancy.[49-51] Assume that the probability $P_{Ll,Mm,\ldots}$, for the creation of l vacancies in the L shell, $0 \leq l \leq 8$, of m vacancies in the M shell, $0 \leq m \leq 18$, etc., is independent of the probability P_{K1} for the creation of one K-shell vacancy. The total probability, P_{K1}^{tot}, for this event is given by the sum over all possible vacancy distributions

$$P_{K1}^{\text{tot}} = \sum_{l,m,\ldots} P_{K1} P_{Ll,Mm,\ldots}. \tag{53}$$

Since

$$\sum_{l,m,\ldots} P_{Ll,Mm,\ldots} = 1,$$

Eq. (53) leads to $P_{K1}^{\text{tot}} = P_{K1}$, which proves that for negligible correlation effects the cross sections developed here $\sigma_K = 2\pi \int P_{K1} b\, db$ include all processes that lead to single K-shell vacancies via direct ionization.

Figure 10 is a universal plot of the K-shell ionization cross sections of $_{13}$Al, prepared according to the low-velocity scaling procedure developed in KI. It corresponds to the limit $c_K \to \infty$ in Eqs. (45) and (47), and $\xi_K = \epsilon_K$. The locus of the data forms a smooth curve that coincides with the function $F_K(y)$ at low velocities. However, as $F_K(y)$ approaches its maximum when $\xi_K > 1$, the data fall systematically above $F_K(y)$. Figure 11 collates our measurements on $_{13}$Al, reduced in the manner of Eq. (47) with $c_K = \frac{3}{2}$. The data follow $F_K(y)$ everywhere within the experimental uncertainties. Theory predicts variations of $F_K(y)$ with Θ_K at intermediate velocities which are less than 10%.[6] They are in the nature of a fine structure not yet resolved by the experiments. Small systematic deviations when $Z_1 \geq 3$ can be accounted for quantitatively by electron capture by the projectile as discussed in connection with Figs. 7–9. Figure 12

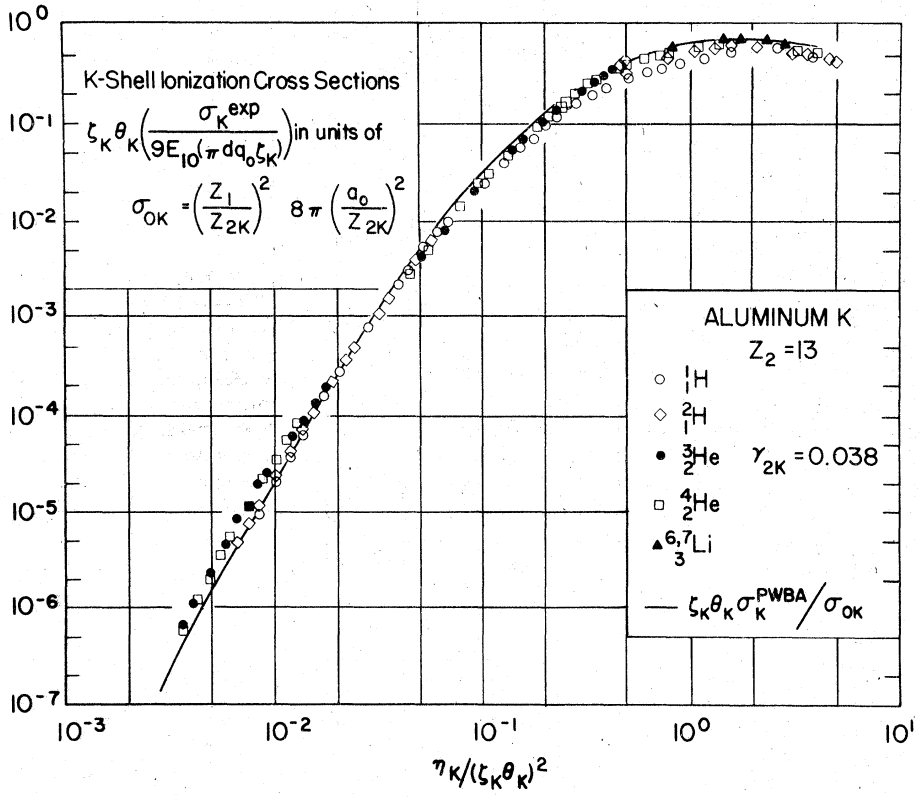

FIG. 11. Universal plot of our $_{13}Al(K)$ ionization cross-section data for six different projectiles $Z_1 \leq 3$ covering the range of energies per nucleon from 0.01 to 10 MeV/amu. The scaling, according to Eq. (47), includes polarization effects. The spread with Z_1 near the maximum can be accounted for through K-electron capture by the projectiles.

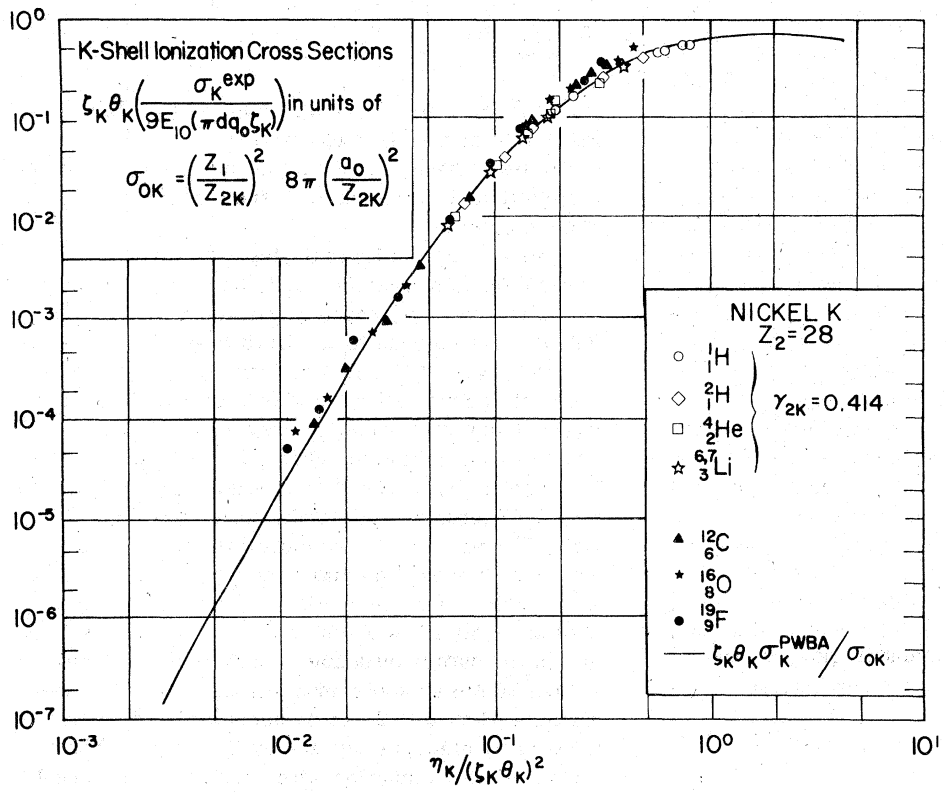

FIG. 12. Same as Fig. 11 for $_{28}Ni(K)$ ionization cross sections for eight different projectiles $Z_1 \leq 9$ using fluorescence yields $\gamma_K = 0.41$ for H, He, Li, and changing $\bar{\gamma}_K$ for C, O, F as presented in Table III and Fig. 3.

shows the analogous plot for $_{28}$Ni.

We conclude that K-shell cross sections for direct Coulomb ionization are predicted accurately and comprehensively through the perturbed stationary-state approximation (CPSS). This new result, consolidated in Eq. (47), incorporates important nonlinear effects into the theory and, thus, goes beyond linear-response theories. Additional contributions come from electron capture, an ionization channel not contained in the theory of direct ionizations. The model-dependent parameter c_K of the theory epitomizes the uncertainties that remain in the transition between the theory of the low-velocity subtractive and the high-velocity additive nonlinear effects in the intermediate particle-velocity regime. They merit further study.

ACKNOWLEDGMENTS

In the course of this work, we have benefited from the encouragement, advice, patience, and critique of many friends and colleagues, for which we are deeply grateful. We are indebted to Grzegorz Lapicki and Kenneth F. Stanton for critical suggestions on the manuscript, and to Anthea Loblack and Linda Kiel for help in its preparation. This research was supported in part by the United States Energy Research and Development Agency. One of us (G.B.) received travel assistance from the Southern Regional Education Board and The North Texas State University Organized Research Funds.

APPENDIX: SAMPLE CALCULATION OF K-SHELL IONIZATION CROSS SECTION

As on previous occasions,[1,2,8] we do not address here the question whether it is meaningful, on a relative scale, to include all contributions however small in the range of the variables chosen, owing to uncertainties in the parameters on which they depend. We simply illustrate the use of the formulas.

Consider the K-shell ionization of $_{13}$Al ($Z_2=13$, $M_2=27$ amu, $\hbar\omega_{2K}=1560$ eV) by a 1.5-MeV/amu $^7_3$Li projectile ($Z_1=3$, $M_1=7$ amu). The primary quantities are

$$\Theta_K=\frac{\hbar\omega_{2K}}{Z_{2K}^2\mathfrak{R}}=\frac{1560\text{ eV}}{(13-0.3)^2\times 13.6\text{ eV}}=0.711\,, \quad \text{(A1)}$$

and by Eq. (2),

$$\eta_K=\left(\frac{v_1}{v_{2K}}\right)^2=\frac{E_1/M_1}{1836Z_{2K}^2\mathfrak{R}}$$
$$=\frac{1.5\text{ MeV}}{1836\times(12.7)^2\times 13.6\text{ eV}}$$
$$=0.372. \quad \text{(A2)}$$

Similarly, by Eq. (1),

$$\xi_K=2\eta_K^{1/2}/\Theta_K=1.72. \quad \text{(A3)}$$

Using $c_K=c_K'=\frac{3}{2}$ gives $g_K(1.72,\ 1.5)=0.152$ from Eqs. (39)–(42) and $I(c_K/\xi_K)=0.415$ by interpolation in Table IV. From these quantities, the value of ζ_K, Eq. (45), is calculated as

$$\zeta_K=1+\frac{2\times 3}{0.711\times 12.7}\left(0.152-\frac{2\times 0.415}{0.711\times(1.72)^3}\right)$$
$$=1+0.664(-0.077)=1-0.0512=0.949, \quad \text{(A4)}$$

so that

$$\zeta_K\Theta_K=0.949\times 0.711=0.675. \quad \text{(A5)}$$

The argument of the function F_K in Eq. (47) becomes

$$\frac{\eta_K}{(\zeta_K\Theta_K)^2}=\frac{0.372}{(0.675)^2}=0.816\,. \quad \text{(A6)}$$

By linear interpolation in Table V of KI, we find $F_K(0.816)=0.640$. Since in our example

$$\sigma_{0K}=8\pi a_0^2\left(\frac{Z_1}{Z_{2K}^2}\right)^2$$
$$=7.04\times 10^{-16}\left(\frac{3}{(12.7)^2}\right)^2\text{ cm}^2$$
$$=2.44\times 10^{-19}\text{ cm}^2, \quad \text{(A7)}$$

and $C_K(\pi\, dq_0\zeta_K)=1$, the direct-ionization cross section, Eq. (47), becomes

$$\sigma_K=2.44\times 10^{-19}\,\frac{0.640}{0.675}\text{ cm}^2=2.31\times 10^{-19}\text{ cm}^2\,. \quad \text{(A8)}$$

For the calculation of σ_K^{EC} according to Eq. (51) we obtain, for $v_1/v_0=Z_{2K}\eta_K^{1/2}=12.7\times(0.372)^{1/2}=7.75$, the value $\mathfrak{N}_f=1-\exp(-0.95\times 7.75/3^{2/3})=0.971$. With $Z_1/Z_{2K}=0.236$, one has

$$\xi_K'=1.72\left[\left(1-\frac{(0.236)^2}{0.711}+\frac{0.372}{0.711}\right)^2+4\left(\frac{0.236}{0.711}\right)^2\right]^{-1/2}$$
$$=1.08\,,$$

so that, from Eqs. (39)–(42) or by linear interpolation in Table V, $g_K(1.08,1.5)=0.318$, which gives $C=0.711[1+(2\times 0.236/0.711)0.318]=0.861$. Collecting $A=3^{1/5}=1.246$, $B=2(1-\frac{4}{3}\times 0.236)=1.37$, and σ_{0K} from Eq. (A7), Eq. (51) yields

$$\sigma_K^{EC} = \frac{0.971(0.236)^3 \times 2.44 \times 10^{-19} \times 2^{16}(0.372)^4}{5\{1.246(0.372)^2 + 2 \times 1.37 \times 0.372[0.861 + (0.236)^2] + [0.861 - (0.236)^2]^2\}^5} \text{ cm}^2 = 0.47 \times 10^{-19} \text{ cm}^2 .$$

When added to Eq. (A8) the calculated ionization cross section becomes 2.78×10^{-19} cm^2. The experimental value from Table I is 8.85×10^3 b/0.038 $= 2.3 \times 10^{-19}$ cm^2. This discrepancy would be removed if $\gamma_{2K} = 0.032$ instead of 0.038.

The calculation for $^2_1$H projectiles of 1.5 MeV/amu is based on the same values of g_K and I, so that now

$$\zeta_K = 1 + \frac{2 \times 1}{0.711 \times 12.7}(-0.077) = 1 - 0.017 = 0.983 \tag{A9}$$

giving

$$\zeta_K \Theta_K = 0.699$$

and

$$\eta_K/(\zeta_K \Theta_K)^2 = 0.761. \tag{A10}$$

From KI, Table V, one has $F_K(0.761) = 0.617$, and the cross section becomes

$$\sigma_K = 7.04 \times 10^{-16}[1/(12.7)^2](0.617/0.699) \text{ cm}^2 = 0.239 \times 10^{-19} \text{ cm}^2. \tag{A11}$$

Electron capture by protons contributions $\sigma_K^{EC} \simeq 0.002 \times 10^{-19}$ cm^2. The experimental ionization cross section from Table I is 7.59×10^2 b/0.038 $= 0.20 \times 10^{-19}$ cm^2; or 0.24×10^{-19} cm^2 if $\gamma_{2K} = 0.032$.

We note that theory and experiment would be in complete agreement for both the Li and H ions if the Al fluorescence yield, γ_K, were equal to 0.032 instead of 0.038 as assumed here. The difference between these two numbers in part may reflect uncertainties in the calibrations to determine the absolute values of σ_K.

The ratio R_{2K}, Eq. (21), becomes

$$R_{2K} = \frac{2.31 \times 10^{-19} \text{ cm}^2}{3^2 \times 0.239 \times 10^{-19} \text{ cm}^2} = 1.07 .$$

Inclusion of electron capture, Eq. (50), yields

$$R'_{2K} = \frac{2.78 \times 10^{-19} \text{ cm}^2}{3^2 \times 0.239 \times 10^{-19} \text{ cm}^2} = 1.29 .$$

The fluorescence-yield-insensitive ratio of experimental values listed in Table II is 1.30 ± 0.03.

*Present address: Dept. of Physics, North Texas State University, Denton, Texas 76203.

[1]G. Basbas, W. Brandt, and R. Laubert, Phys. Rev. A 7, 983 (1973), henceforth referred to as KI.

[2]W. Brandt and G. Lapicki, Phys. Rev. A 10, 474 (1974), henceforth referred to as LI.

[3]W. Brandt, in *Proceedings of the International Conference on Inner-shell Ionization Phenomena and Future Applications, Atlanta, Georgia, 1972,* edited by R. W. Fink, S. T. Manson, M. Palms, and P. V. Rao (U.S. AEC CONF-720404, Oak Ridge, Tenn., 1973), p. 948; *Atomic Physics 3* (Plenum, New York, 1973), p. 155; W. Brandt, R. Laubert, and I. Sellin, Phys. Lett. 21, 518 (1966); G. Basbas, W. Brandt, and R. Laubert, Phys. Lett. 34A, 277 (1971).

[4]G. Basbas, W. Brandt, and R. H. Ritchie, Phys. Rev. A 7, 1971 (1973).

[5]G. Bissinger, J. M. Joyce, and H. W. Kugel, Phys. Rev. A 14, 1375 (1976).

[6]G. S. Khandelwal, B. H. Choi, and E. Merzbacher, At. Data 1, 103 (1969) (K shells). The range of this table has been extended by R. Rice, G. Basbas, and F. D. McDaniel, At. Data Nucl. Data Tables (to be published).

[7]B. H. Choi, F. Merzbacher, and G. S. Khandelwal, At. Data 5, 291 (1973) (L shells).

[8]J. C. Ashley, R. H. Ritchie, and W. Brandt, Phys. Rev. B 5, 2393 (1972); Phys. Rev. A 8, 2402 (1973); 10, 737 (1974).

[9]J. S. Hansen, H. U. Freund, and R. W. Fink, Nucl. Phys. A 142, 604 (1970); V. W. Slivinsky and P. J. Ebert, Phys. Rev. A 5, 1581 (1972).

[10]J. H. Scofield, Phys. Rev. 179, 9 (1969).

[11]E. J. McGuire, Phys. Lett. 33A, 288 (1970).

[12]The Be mass absorption coefficient $\mu = 188$ cm^2/g for Al(K) x rays resulted from an interpolation between μ values quoted by G. L. Clark, in *Handbook of X-rays*, edited by E. F. Kaelble (McGraw-Hill, New York, 1967), Chap. 1, p. 27.

[13]ABACUS-2 calculation kindly performed by E. H. Auerbach, Brookhaven National Laboratory (private communication).

[14]P. Richard, in *Proceedings of the International Conference on Inner-shell Ionization Phenomena and Future Applications, Atlanta, Georgia, 1972,* edited by R. W. Fink, S. T. Manson, M. Palms, and P. V. Rao (U.S. AEC CONF-720404, Oak Ridge, Tenn., 1973), p. 1641.

[15]M. J. Saltmarsh, A. van der Woude, and C. A. Ludemann, Phys. Rev. Lett. 29, 329 (1972).

[16]D. Burch and P. Richard, Phys. Rev. Lett. 25, 983 (1970).

[17]E. J. McGuire, Phys. Rev. 185, 1 (1969).

[18]W. Bambynek, B. Crasemann, R. W. Fink, H. U. Freund, H. Mark, C. D. Swift, R. E. Price, and P. Venugopala Rao, Rev. Mod. Phys. 44, 716 (1972).

[19]W. Brandt and R. Laubert, Phys. Rev. A 11, 1233 (1974), and references cited therein.

[20]J. M. Khan and D. L. Potter, Phys. Rev. 133A, 890 (1964); J. M. Khan, D. L. Potter, and R. D. Worley, *ibid.* 139A, 1735 (1965).

[21]P. Komarek, Acta Phys. Austriaca 27, 369 (1968).

[22]B. Sellers, F. A. Hanser, and H. H. Wilson, Phys. Rev. 182, 90 (1969).

[23]G. Lapicki and W. Losonsky, Phys. Rev. A 15, 896

(1977), and references cited therein.
[24]J. Bang and J. M. Hansteen, K. Dan. Vidensk. Selsk. Mat. Fys. Medd. 31, No. 13 (1959).
[25]K. W. Hill and E. Merzbacher, Phys. Rev. A 9, 156 (1974).
[26]From J. C. Ashley, V. E. Anderson, R. H. Ritchie, and W. Brandt, Z_1^3 *Effects in the Stopping Power of Matter for Charge Particles: Tables of Functions*, Document No. 02195, (National Auxiliary Publication Service, 440 Park Avenue South, New York, N.Y. 10016, 1974). Interpolation formula, Eq. (27), courtesy G. Lapicki.
[27]J. D. Jackson and R. L. McCarthy, Phys. Rev. B 6, 4131 (1972).
[28]H. H. Andersen, J. F. Bak, H. Knudsen, P. Møller Peterson, and B. R. Nielsen, Nucl. Instrum. Methods 140, 537 (1977).
[29]J. Lindhard, Nucl. Instrum. Methods 132, 1 (1976).
[30]H. A. Bethe and E. E. Salpeter, in *Handbuch der Physik*, edited by S. Flügge (Springer, Berlin, 1957), Vol. 35, p. 389ff.
[31]J. U. Andersen, E. Laegsgaard, M. Lund, and C. D. Moak, Nucl. Instrum. Methods 132, 507 (1976).
[32]L. Kocbach, Phys. Norv. 8, 187 (1976).
[33]P. A. Amundsen, J. Phys. B 10, 2177 (1977).
[34]S. R. Wilson, F. D. McDaniel, J. R. Rowe, and J. L. Duggan, Phys. Rev. A 16, 903 (1977).
[35]O. N. Jarvis, C. Whitehead, and M. Shah, Phys. Rev. A 5, 1198 (1972).
[36]N. Stolterfoht, D. Schneider, and K. G. Harrison, Phys. Rev. A 8, 2363 (1973).
[37]J. F. Reading, A. L. Ford, and E. Fitchard, Phys. Rev. Lett. 36, 573 (1976).
[38]Y. Awaya, K. Izumo, T. Hamada, N. Okano, T. Takahashi, A. Hashizume, Y. Tendow, and T. Katou, Phys. Rev. A 13, 992 (1976), and references cited therein.
[39]G. Lapicki, F. D. McDaniel, and G. Basbas, Bull. Am. Phys. Soc. 22, 585 (1977), and to be published.
[40]This expression approximates the results of the theory of effective charge numbers Z_1^{eff} of moving ions in the statistical model given by W. Brandt, in *Proceedings of the Fifth International Conference on Atomic Collisions in Solids, Gatlinburg, Tennessee, 1973*, edited by S. Datz, B. R. Appelton, and C. B. Moak (Plenum, New York, 1975), p. 261ff.
[41]V. S. Nikolaev, Zh. Eksp. Teor. Fiz. 51, 1203 (1966) [Sov. Phys.-JETP 24, 847 (1977)].
[42]Courtesy G. Lapicki.
[43]W. Brandt and R. Laubert, Phys. Rev. Lett. 24, 1039 (1970).
[44]R. Laubert and W. Losonsky, Phys. Rev. A 14, 2043 (1976), and references cited therein.
[45]G. Basbas, in *Abstracts of Papers, Ninth International Conference on the Physics of Electronic and Atomic Collisions*, edited by J. R. Risley and R. Geballe (Washington U.P., Seattle, 1975), p. 502.
[46]F. K. Chen, G. Lapicki, R. Laubert, S. B. Elston, R. S. Peterson, and I. A. Sellin, Phys. Lett. 60A, 292 (1977).
[47]W. Losonsky, Phys. Rev. A 16, 1312 (1977).
[48]A. R. Knudson, D. J. Nagel, P. G. Burkhalter, and K. L. Dunning, Phys. Rev. Lett. 26, 1149 (1971).
[49]J. F. Reading, Phys. Rev. A 8, 3262 (1973).
[50]J. H. McGuire and J. R. Macdonald, Phys. Rev. 11, 146 (1975).
[51]G. Basbas, Bull. Am. Phys. Soc. 20, 675 (1975).